A new aerodynamic phenomenon and its effects on the design of ultra-high cylindrical towers

Dissertation

submitted to and approved by the

Department of Architecture, Civil Engineering and Environmental Sciences
University of Braunschweig – Institute of Technology

and the

Department of Civil and Environmental Engineering
University of Florence

in candidacy for the degree of a
Doktor-Ingenieurin (Dr.-Ing.) /
Dottore di Ricerca in Mitigation of Risk due to Natural Hazards on Structures and Infrastructures[*)]

by
Francesca Lupi
Born 21 April 1984
from Prato, Italy

Submitted on	6 March 2013
Oral examination on	23 April 2013
Professorial advisors	Prof. Claudio Borri Prof. Udo Peil Prof. Hans-Jürgen Niemann

2013

*) Either the German or the Italian form of the title may be used.

Acknowledgments

First of all, I would like to thank my advisors, Prof. Claudio Borri, Prof. Udo Peil and Prof. Hans-Jürgen Niemann. A special thanks to Prof. Borri, for his continuous support and interest in this work and for his many ideas, which have suggested further new hints of research. All my gratitude to Prof. Peil, because his advice motivated me to pursue the original contributions of this work. I will always be grateful to Prof. Niemann for the time and the constancy he dedicated to our discussions. The strong motivation he transmitted has been during these years my encouragement and support to always go deeper and deeper in this research.

I would also like to acknowledge Prof. Borri and Prof. Peil for the efforts they made for the success of our International Doctoral Course. This International PhD has been an intensive sequence of many different experiences which have really enriched me.

I am grateful to my colleagues in Florence for their support and discussions during these years. I would like to thank Prof. Luca Facchini for the ideas he exchanged with me and the interesting new studies which could develop from this research.

I express my gratitude to all the colleagues at the TU Braunschweig for their kind hospitality and exchange of ideas. I especially thank Dr. Mathias Clobes for the fruitful discussions we had.

I acknowledge Mrs Serena Cartei and Mrs Yvonne Wissmann for their kind support and many efforts in the organization.

I will never forget the support and the friendly atmosphere I experienced at WiSt Ruhr University Bochum, where I spent many months during this work. First of all, I would like to thank Prof. Rüdiger Höffer for his kind hospitality at the Institute and the opportunity he gave me to work in the wind tunnel. Mrs Christa Hoogterp and Mr Volkmar Görnandt have always been so kind and helpful in the organization of my stay in Bochum, I appreciated it so much. A special thanks is for Mr Reinhard Elke and Mr Uwe Wagner, for their indispensable guidance and kind support during the wind tunnel experiments at WiSt. I would also like to express my gratitude to all the colleagues I met there, their company has been so important during the hardest periods of this work.

I express my gratitude to Lorenzo Procino and Alessandra Borsani for the support during the wind tunnel tests at CRIACIV.

I deeply acknowledge Simone Salvadori and Alessandro Mattana of Prof. Martelli's research group at the University of Florence for their cooperation in the numerical simulations. I also thank Gabriele Barbanti and Giulio Vita for their kind help.

I owe very much to my family, that I always felt close even living abroad and encouraged me in every moment of my life to purse my goals.

Abstract

The dissertation addresses the design of ultra-high towers in the atmospheric boundary layer under the wind action and has a special application for Solar Updraft Power Plants (SUPPs). They represent a highly sustainable natural resource for electric power generation, based on a combined sun-wind energy solution.

The object of the investigation is a 1-km tall solar updraft tower, made of reinforced concrete and stiffened along the height by stiffening rings. Stiffening rings are usually introduced in the design of solar updraft towers in order to reduce their structural vulnerability to the wind action by enhancing a beam-like behaviour. However, wind tunnel experiments – which were performed for the first time on such a structure within this research – showed that the presence of ring beams along the height of the tower modifies the aerodynamics of the flow around the circular cylinder and creates a bi-stable and asymmetric load condition, which does not disappear even at moderately high Reynolds numbers. This phenomenon is new and unknown. Similar effects were observed around circular cylinders (without rings) in the critical range of the Reynolds number and around two side-by-side cylinders, but the conditions of occurrence and the physical reasons were profoundly different.

The discovery of the existence of such a bi-stable and asymmetric load condition induced by ring beams along the height of a finite length circular cylinder, its interpretation, as well as the cross-checked experimental evidence in different wind-tunnel laboratories confirmed also by numerical simulations, are the original contributions of this work. Then, the effect is quantified on the structural response. The bi-stable asymmetric load on the structure did not result to be a prohibitive load condition for solar updraft towers and the magnitude of the effect depends on the number and/or on the size of the rings. Mitigation strategies are then proposed in the work. Furthermore, the dissertation evaluates the shell response to the stochastic wind loading process, especially in the vicinity of the ring beams, and provides to the designer a general unified simple tool to define design wind loads for quasi-static calculations of ultra-high towers in any atmospheric boundary layer flow.

Sommario

La tesi riguarda il progetto di torri di altezza straordinaria nello strato limite atmosferico, soggette all'azione del vento. Un particolare campo di applicazione è quello degli impianti di torri solari ad aspirazione, "Solar Updraft Power Plants" (SUPPs). Questi rappresentano una nuova e sostenibile risorsa di energia rinnovabile, basata sullo sfruttamento combinato di energia solare ed eolica.
L'oggetto dello studio è una torre solare ad aspirazione in calcestruzzo armato alta 1 km e irrigidita lungo l'altezza da travi ad anello. Queste sono normalmente utilizzate nel progetto di torri solari per ridurre la vulnerabilità all'azione del vento, in quanto la loro presenza garantisce un comportamento strutturale predominante a trave. Tuttavia, gli esperimenti in galleria del vento – effettuati per la prima volta su una struttura di questo tipo nell'ambito del presente lavoro – hanno mostrato che gli anelli lungo l'altezza della torre modificano l'aerodinamica del flusso e creano attorno al cilindro una condizione di carico bistabile e non simmetrico. L'effetto non scompare a numeri di Reynolds moderatamente elevati ed il fenomeno è nuovo e sconosciuto. Effetti simili sono stati osservati attorno a cilindri circolari (senza anelli) nell'intervallo critico del numero di Reynolds e attorno a due cilindri affiancati. Tuttavia, le condizioni in cui si verificano e il principio fisico sono profondamente diversi.
La scoperta dell'esistenza di una tale condizione di carico bistabile e non simmetrica indotta da anelli disposti lungo l'altezza di un cilindro circolare di altezza finita, la sua interpretazione, così come l'evidenza sperimentale in gallerie del vento diverse e la sua conferma numerica, sono i contributi originali di questo lavoro. L'effetto è poi quantificato in termini di risposta strutturale. La condizione di carico bistabile e non simmetrica non risulta proibitiva per il progetto di torri solari e la sua incidenza dipende dal numero e/o dalla dimensione degli anelli. Strategie di mitigazione dell'effetto sono proposte nel lavoro. Inoltre, la tesi studia la risposta della torre al carico del vento, specialmente vicino agli anelli di irrigidimento. Infine, la tesi fornisce al progettista uno strumento semplice e di validità generale per definire i carichi di progetto dell'azione del vento, utilizzabili nel calcolo quasi-statico della risposta di torri di altezza elevata nello strato limite atmosferico.

Zusammenfassung

Die hiermit vorgelegte Doktorarbeit befasst sich mit der Einwirkung des natürlichen Windes auf ultra-hohe Turmbauwerke, die weit in die atmosphärische Grenzschichtströmung hineinreichen. Die Türme von Aufwindkraftwerken stehen hierbei im Vordergrund. Derartige Kraftwerke ermöglichen eine schadstofffreie Erzeugung elektrischer Energie. Sie stellen eine sehr nachhaltige Technologie dar, die thermische Energie der Sonne in Strömungsenergie umwandelt, die ihrerseits mit Hilfe von Turbinen als elektrische Energie nutzbar gemacht wird.

Als Untersuchungsgegenstand der Arbeit dient beispielhaft ein 1 km hoher Aufwindturm. Das Tragwerk ist als Stahlbetonschale, die durch Aussteifungsringe verstärkt ist, konzipiert. Die Versteifung vermindert die durch die Einwirkung von Winddrücken erzeugten Beanspruchungen, indem sie ein stabartiges Tragverhalten bewirkt. Erstmalig wurden im Rahmen dieser Forschungen Windkanalversuche an Aufwindtürmen durchgeführt. Sie zeigten, dass die außenliegenden Versteifungsringe die aerodynamischen Eigenschaften des Turmes im Vergleich zu einem endlichen Kreiszylinder ohne Ringe erheblich verändern: Zwischen den Ringen entsteht abschnittsweise ein unsymmetrischer, bi-stabiler Strömungs- und Belastungszustand, der bis zu den höchsten untersuchten Reynoldszahlen zu beobachten ist. Ähnliche Effekte sind zwar auch bei einem Zylinder ohne Ringe bekannt, sie sind dort jedoch auf einen schmalen Bereich kritischer Reynoldszahlen beschränkt. Ebenfalls zeigen sich derartige Strömungszustände bei 2 nebeneinanderliegenden Zylindern bei bestimmten Abstandsverhältnissen. Die physikalischen Ursachen des hier bei Zylindern mit Ringen erstmalig beobachteten Phänomens sind jedoch grundsätzlich unterschiedlich.

Originäre Beiträge der Arbeit sind die Entdeckung der abschnittsweise unsymmetrischen, bi-stabilen Windbelastung, die Bestätigung des experimentellen Befundes durch Versuche in einem zweiten Windkanallaboratorium und durch numerische Simulationen, sowie schließlich die Deutung des Phänomens. Weiterhin wird die Auswirkung der zusätzlichen Windbelastung auf die Strukturbeanspruchungen untersucht. Es wird gezeigt, dass Anzahl und Breite der Ringbalken die Größe des Lasteffekts bestimmen; Maßnahmen zu seiner Minderung werden entwickelt. Insgesamt bleiben die Zusatzbeanspruchungen beherrschbar. Abschließend befasst sich die Arbeit mit den Tragwerksbeanspruchungen infolge des stochastischen Windlastprozesses, insbesondere mit den Störungen des Membranzustands in der Umgebung der Ringsteifen. Für die Tragwerksplanung werden verallgemeinerte Wind-Ersatzlasten entwickelt, die geeignet sind, als Grundlage zur Berechnung der statischen und quasi-statischen Beanspruchungen ultra-hoher Türme in beliebiger atmosphärischer Grenzschichtströmung zu dienen.

Table of Contents

List of Figures

List of Tables

List of Symbols

A_c = area of the chimney

A_{coll} = area of the collector

C_D = drag coefficient

$C_{D,m}$ = mean drag coefficient

$C_{D,\ peak}$ = peak drag coefficient

$C_{D,\ \sigma}$ = standard deviation of the drag coefficient

C_L = lift coefficient

$C_{L,m}$ = mean lift coefficient

$C_{L,\ \sigma}$ = standard deviation lift coefficient

Co = co-spectrum

C_p = pressure coefficient (external)

$C_{p,air}$ = specific heat capacity of air

$C_{p,b}$ = base pressure coefficient

$C_{p,h}$ = pressure coefficient at φ_h

$C_{p,i}$ = internal pressure coefficient

$C_{p,m}$ = mean pressure coefficient

$C_{p,max}$ = maximum pressure coefficient

$C_{p,min}$ = minimum pressure coefficient

C_{pp} = decay coefficient of ρ_p

C_{uu} = decay coefficient of ρ_u

$C_{p,\sigma}$ = standard deviation of pressure coefficient

$C_{p,\sigma,BI}$ = standard deviation of pressure coefficient, body-induced part

$C_{p,\sigma,TI}$ = standard deviation of pressure coefficient, turbulence-induced part

D = diameter

D = damping matrix

D_{coll} = diameter of the collector

E = voltage measured by hot-wire anemometers (either E_a or E_{corr})

E_a = voltage measured by hot-wire anemometers, without temperature correction

E_{corr} = voltage measured by hot-wire anemometers, with temperature correction

EaR = element at risk

F_m = mean (drag) force

$\mathbf{F}_r$ = friction force (vector)

F_x = friction force along x-axis

F_y = friction force along y-axis

F_z = friction force along z-axis

F_σ = rms (drag) force

G = [1)] solar radiation (Chapter 1); [2)] gradient wind speed (Chapter 2)

H = height of the tower = 1000 m

H/D = aspect ratio

H&D = Harris and Deaves model

I_F = intensity of force (standard deviation / mean value)

I_p = intensity of pressure (standard deviation / mean value)

$I_{p,TI}$ = intensity of pressure (standard deviation / mean value), turbulence-induced part

I_u = turbulence intensity (along wind component)

K = stiffness matrix

K_0 = Kolmogorov parameter

L = [1)] mixing length; [2)] length scale of mid-latitude synoptic systems

L_f = eddy formation region in the wake of a cylinder

L_{LIFT} = correlation length of C_L

L_{pz} = pressure correlation length (z direction)

L_{ux}, L_{uy}, L_{uz} = integral length scales of the along-wind velocity component

L_{VS} = correlation length of vortex shedding lift

L_{vx}, L_{vy}, L_{vz} = integral length scales of the across-wind velocity component

L_{wx}, L_{wy}, L_{wz} = integral length scales of the vertical component of wind velocity

M = mass matrix

M_D = bending moment in the along-wind direction

$M_{D,m}$ = mean bending moment in the along-wind direction

$M_{D,peak}$ = peak bending moment in the along-wind direction

$M_{D,\sigma}$ = rms bending moment in the along-wind direction

$M_{D,}\sigma_B^2$ = variance of M_D, quasi-static part (resonance not included)

$M_{D,}\sigma_B^2 + \sigma_R^2$ = variance of M_D, including resonance

M_L = bending moment in the across-wind direction

$M_{L,m}$ = mean bending moment in the across-wind direction

$M_{L,peak}$ = peak bending moment in the across-wind direction

$M_{L,\sigma}$ = rms bending moment in the across-wind direction

$M_{L,}\sigma_B^2$ = variance of M_L, quasi-static part (resonance not included)

$M_{L,}\sigma_B^2 + \sigma_R^2$ = variance of M_L, including resonance

$M_{res,m}$ = mean resultant bending moment

$M_{res,peak}$ = peak resultant bending moment

$M_{res,\sigma}$ = rms resultant bending moment

$M_{res,}\sigma_B^2$ = variance of M_{res}, quasi-static part (resonance not included)

$M_{res,}\sigma_B^2 + \sigma_R^2$ = variance of M_{res}, including resonance

N = number of time steps

P_{el} = electric output

P_{tot} = power of the power plant

Qu = quad-spectrum

$\dot{Q}$ = heat increase in the collector

R = radius

Re = Reynolds number

Re_{cr} = critical Reynolds number

Re_e = effective Reynolds number

Ro = Rossby number

R_u = autocovariance function of u

S = [1)] power spectral density function; [2)] generic effect in the tower response (either n_{11}, n_{22}, …)

S_{cr} = Scrouton number

S_t = Strouhal number

SUPP = Solar Updraft Power Plant

T_0 = ambient temperature

T_a = ambient temperature during acquisition of hot-wire signals

T_{ux} = integral time scale

T_w = hot-wire operational temperature = 250°

T/D = centre-to-centre transverse pitch ratio in side-by-side cylinders

U = wind velocity in the along wind direction

U_{cr} = critical velocity

U_{FS} = full-scale velocity

U_g = gradient wind, component along x-axis (reference system as specified in the context)

U_m = mean along wind component

$U_{m,\infty}$ = mean along wind component in the undisturbed flow

U_{pra} = Prandtl velocity, i.e. wind tunnel velocity at the Prandtl tube

U_{ref} = reference wind velocity

U_{WT} = wind tunnel velocity

$\mathbf{V}$ = velocity vector

V_b = basic wind velocity at 10 m height (code denomination)

V_c = flow speed in the chimney

$V_{c,max}$ = maximum flow speed in the chimney

V_g = gradient wind, component along y-axis (reference system as specified in the context)

c = ratio between L_{uz} and L_{pz}

cov_D = covariance matrix of drag force

f_c = Coriolis parameter

f_{sz} = correction factor on C_D for boundary layer flow (ESDU)

g = gravitational acceleration

h = gradient height

k = von Karman constant (k = 0.4)

k_F = peak factor of the force (k_F = 3.5)

ks = thickness of ribs on the wind tunnel model

k_P = peak factor of the velocity (k_P = 3.5)

k_{pw} = pressure withdrawal factor for the turbines

$\dot{m}$ = mass flow rate

$m_{i,e}$ = equivalent mass of the structure per unit length, i^{th} vibration mode

m_{11} = bending moment in the circumferential direction per unit length ($m_{11,m}$, $m_{11,\sigma}$, $m_{11,peak}$, see $n_{11,...}$)

m_{22} = bending moment in the meridional direction per unit length ($m_{22,m}$, $m_{22,\sigma}$, $m_{22,peak}$, see $n_{11,...}$)

n = frequency

n_s = vortex shedding frequency

n_1 = first eigenfrequency

n_{11} = internal force in the circumferential direction per unit length

$n_{11,m}$ = mean value of n_{11}

$n_{11,\sigma}$ = mean value of n_{11}

$n_{11,peak}$ = peak value of n_{11}

n_{22} = internal force in the meridional direction per unit length ($n_{22,m}$, $n_{22,\sigma}$, $n_{22,peak}$, see $n_{11,...}$)

p = pressure

p_m = mean pressure

p_σ = standard deviation of the pressure p

$p_{\sigma,BI}$ = standard deviation of the pressure p, body-induced part

$p_{\sigma,TI}$ = standard deviation of the pressure p, turbulence-induced part

q_m = mean velocity pressure

q_{peak} = peak velocity pressure

t = time

u = along-wind component

u_* = friction velocity

v = across-wind component

w = [1)] vertical wind component; [2)] width of the ring beams

x = along-wind direction in the wind tunnel

y = across-wind direction in the wind tunnel

z_0 = roughness length

z = vertical coordinate

z' = downwards vertical coordinate with origin at z = H (tower top)

z_{ref} = reference height

ΔC_p = pressure recovery

Δp_d = pressure difference, dynamic component

Δp_s = pressure difference, static component

Δp_{tot} = pressure difference, static + dynamic

ΔT = temperature increase/decrease

Ω = angular velocity of Earth rotation, magnitude

$\boldsymbol{\Omega}$ = angular velocity of Earth rotation, vector

α = exponent of mean wind profile by using power law

δ = [1)] thickness of the boundary layer; [2)] logarithmic decrement

ε = dissipation

ξ = modal damping ratio

η = [1)] efficiency of the power plant (Chapter 1); [2)] influence coefficient (Chapter 7)

η_c = efficiency of the chimney

η_{coll} = efficiency of the collector

η_{turb} = efficiency of the turbines

θ = phase angle

ϑ_0 = maximum angle of turn due to Ekman spiral

λ_F = frequency scale factor (wind tunnel and full scale)

λ_L = length scale factor (wind tunnel and full scale)

λ_R = roughness factor in the definition of Re_e

λ_T = [1)] time scale factor (wind tunnel and full scale); [2)] turbulence factor in the definition of Re_e

λ_V = velocity scale factor (wind tunnel and full scale)

μ = dynamic viscosity

ν = kinematic viscosity

ρ = [1)] mass density of air; [2)] cross-correlation coefficient

ρ_0 = mass density of air at 20°

ρ_a = mass density of air outisde the chimney

ρ_c = mass density of air inside the chimney

ρ_{coll} = mass density of air inside the collector

ρ_D = correlation matrix of drag force

ρ_p = cross-correlations of p

ρ_u = cross-correlations of u

σ = standard deviation

σ^2 = variance

σ_B = standard deviation of background response

σ_u = standard deviation of u

$\sigma_{u,\infty}$ = standard deviation of along wind component in the undisturbed flow

σ_v = standard deviation of v

σ_w = standard deviation of w

τ = shear stresses

ϕ = latitude

φ = circumferential angle

φ_h = angle of separation

φ_{min} = angle of $C_{p,min}$

ω = circular frequency

^{EXP} = experimental result

^{LM} = loading model

‘ = fluctuating component

Chapter 1. **Introduction**

The design of ultra-high structures in the atmospheric boundary layer is a pioneering field of study, where research and application complement each other. The recent construction of super-tall skyscrapers – more than 800 m in height – represents today the highest synthesis of these efforts. This thesis proposes and investigates a new context of application – the Solar Updraft Power Plant Technology – a highly sustainable natural resource for electric power generation. This chapter introduces the technology, the working principle and the aim of the research.

1.1 The Solar Updraft Power Plants technology

The Solar Updraft Power Plants technology (SUPPs) produces renewable energy by sun-wind energy harvesting. Solar radiation is an inexhaustible input, which is converted into electric power through the natural updraft of heated air in a very high chimney.

Peculiar characteristics of this technology are its long lifetime (more than 100 years), its very low costs of operation, the no-need of water for power generation and the absence of pollutant emissions (if one incorporates the CO_2 emissions during construction, one ends up with a few grams of CO_2 per kWh of produced electricity (Backström et al., 2008)).

A SUPP consists of three elements (Figure 1.2): the collector, the turbine(s) with coupled generators as power conversion unit and the solar tower. The collector is a large glass-covered area where the visible and the ultraviolet wavelengths of the solar radiation heat the ground and consequently warm up the air under the roof, through the mechanism of natural convection. Meanwhile, the infrared wavelengths warm up the energy storage layer made of the soil itself, stones or, in case, water. Such an energy storage allows night operation. Then, the heated, less dense air rises up into the chimney of the plant, thereby drawing in more air at the collector perimeter and thus initiating forced convection. The driving force or potential that causes air to flow through the solar tower is the pressure difference between a column of cold air outside and a column of hot air inside the chimney. The stream of warm air turns the turbines at the chimney foot and in the power conversion unit the kinetic energy of the flow is transformed into electric power.

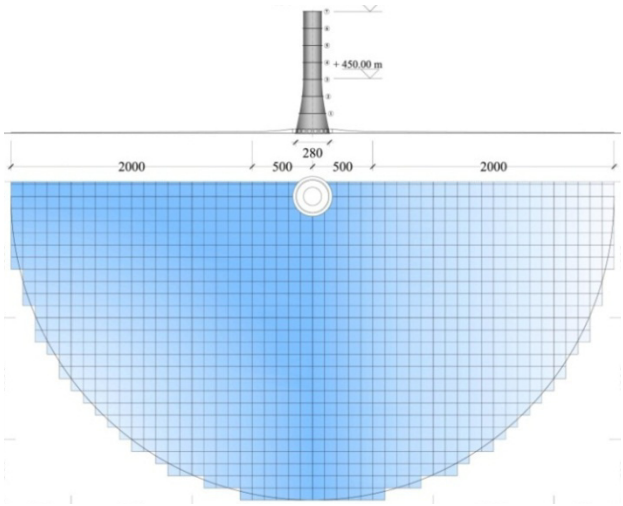

Figure 1.1 View of a Solar Updraft Power Plant

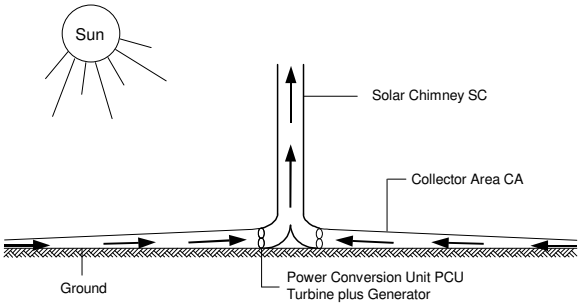

Figure 1.2 Working principle

The production of energy is proportional to the volume of the cylinder with the height of the tower and the diameter of the collector (Schlaich et al., 2005). For this reason, provided sufficiently high solar radiation input (e.g. 2000 kWh/m^2 or even more), very good efficiency of the power plant can be reached with extra-large dimensions of the tower and/or the collector.

A map of the yearly solar radiation distribution is shown in Figure 1.3. It suggests the most suitable locations for SUPPs around the world (Pretorius, 2007). In those areas, a plant with a collector diameter of 7 km and with solar tower height of 1500 m is estimated to deliver a maximum (peak) electricity power of 400 MW (Pretorius&Kröger, 2006). This assumption has been also assessed, both experimentally and theoretically for a wide range of plant geometries, as a reasonable global assumption (Fluri, 2008).

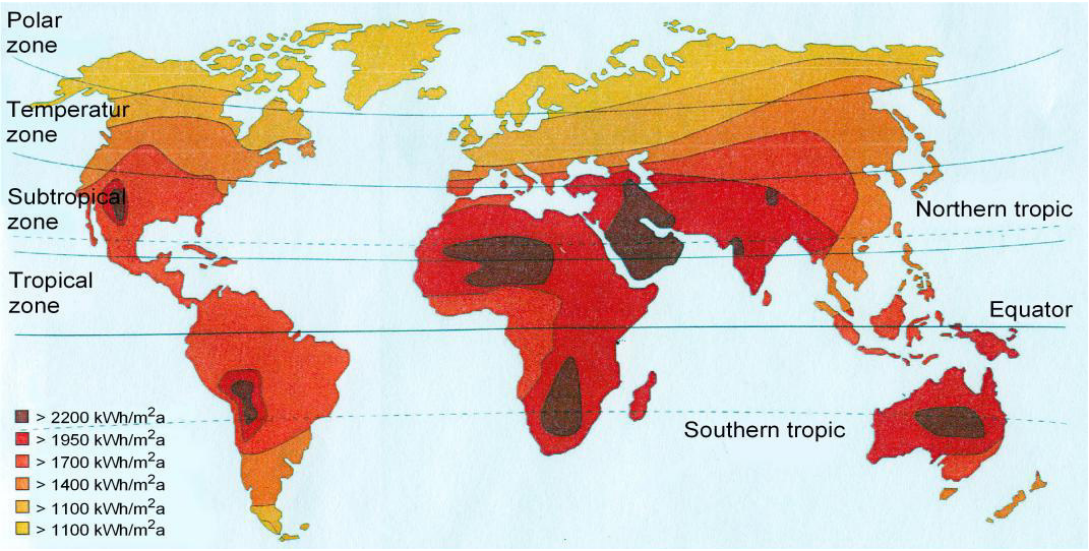

Figure 1.3 Solar radiation input (Pretorius, 2007)

1.2 Historical review

The paternity of the SUPPs idea is commonly attributed to the Spanish army colonel I. Cabanyes (Cabanyes, 1903), although a patent for “an improved temperature differential air motor” was invented even earlier – in 1896 – by A. R. Bennett (Bennett, 1896), a prototype of which is shown at the Science Museum in London.

The apparatus proposed by Cabanyes consisted of an air-heater attached to a house with a chimney. Inside the house, there was a wind propeller for electricity production (Figure 1.4).

Another early description of the SUPP principle can be found in the work of the German author Hanns Günther (Günther, 1931). The idea of the author was a solar chimney on the slope of a mountain (Figure 1.5). The very high air speed could deliver an enormous amount of energy, which could be extracted by means of wind turbines.


AÑO V.—Tomo 2. 25 de Agosto de 1903. Núm. 4

La Energia Eléctrica

REVISTA GENERAL DE ELECTRICIDAD Y SUS APLICACIONES

PUBLICACIÓN QUINCENAL ILUSTRADA

SUMARIO

PROYECTO DE MOTOR SOLAR

Figure 1.4 Article of Isidoro Cabanyes, published on “La Energia Electrica” (Cabanyes, 1903).

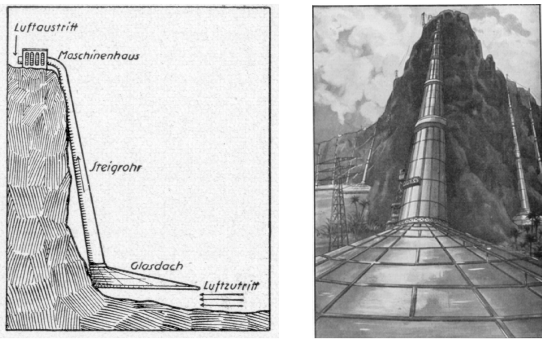

Figure 1.5 A solar chimney on the slope of a high mountain. (Günther, 1931)

Around 1975, a series of patents were granted to the US engineer R.E. Lucier in countries with deserts suitable for SUPPs, like Australia, Canada, Israel and the US. These patents concerned: "Apparatus for converting Solar to Electrical Energy", "Utilization of Solar Energy", "System and Apparatus for Converting Solar Heat to Electrical Energy", "System for converting solar heat to electrical energy".

Jörg Schlaich, Rudolf Bergermann and their team have been very active in developing and spreading the Solar Updraft Power Technology. Their first idea – as reported in (Schlaich, 2010) – goes back to 1972, when they were invited by the power industry to develop a large scale cooling tower for dry cooling. A new question arose among them, whether the natural updraft which is produced in such chimney tubes could not be utilized to produce electricity, provided an additional “fire” at the base of the chimney tube. And why not to use solar radiation and collect solar warm air by means

of a large greenhouse roof? All of that resulted, in 1979, in what they called the "Solar Chimney" (Schlaich, 2010). As they said, Schlaich and his team developed the whole idea on their own, and only some years later they got hold of the paper written in 1931 by Günther, describing the similar basic principle of the solar updraft tower. In 1980, thanks to a grant by the German Ministry for Research and Technology, J. Schlaich built a solar tower prototype with a maximum power output of 50 kW in Manzanares (Spain), in order to test the new technology and confirm analytical results through experimental data (Figure 1.6). "The aim of this research project was to verify, through field measurements, the performance projected from calculations based on theory, and to examine the influence of individual components on the plant' output and efficiency under realistic engineering and meteorological conditions" (Schlaich, 1995). The chimney was a cylindrical tube of 195 m in height and 10 m in diameter. It was surrounded by a collector of 240 m in diameter. The design was only made for experimental purposes, i.e. to collect measurements for a period of three years. The plant was intended to be removed without trace after that. Being a temporary structure, the chimney was made of a corrugated metal sheeting, whose thickness was only 1.25 mm and which could be used again after the experiment. In fact, the original plan was to take measurements in 1981 and 1982 and dismantle the structure in 1983, after three years from the construction, since the grant did not permit regular corrosion protection especially for the stay-cables. Anyway, years passed away permitting them to take more measurements. The chimney lasted for eight years, until spring 1989, when the cables broke in a storm and the chimney fell down. When it happened, the necessary measurements had largely been completed. Experimental results were very promising, a detailed analysis can be found in (Schlaich, 1995).

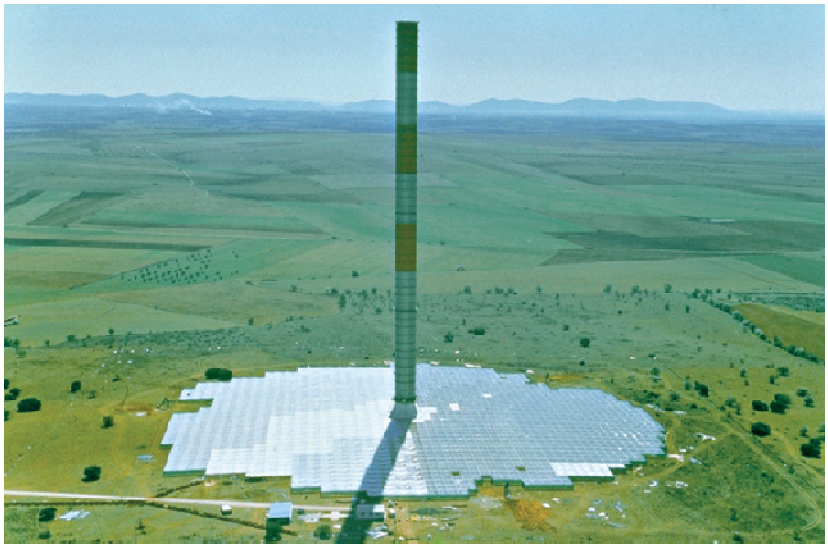

Figure 1.6 J. Schlaich's prototype in Manzanares/Spain (Schlaich, 1995)

In 1987, Pasumarthi and Sherif erected a small prototype installation in California and published the first thermo-mechanical plant model (Pasumarthi&Sherif, 1997).
A recent experimental investigation of the solar collector temperature field on a 9 m tall prototype with sloped collector is currently being performed by Kalash et others, 2012. A complete up-to-date bibliography of the latest worldwide studies can be found in the Proceedings of both the 2nd and the 3rd International Conferences on SUPPs (STPT2010, SUTPT 2012).
Up to now, several projects of large SUPPs have been developed in arid zones all over the world, but none of them has come to realization. In 2008, the Namibian government approved a proposal for the construction of a 400 MW solar chimney called the 'Greentower'. The tower was planned to be 1.5 kilometres tall and 280 m in diameter, and the base consisted of a 37 square kilometres greenhouse. In recent years EnviroMission (Australia) proposed a 200 MW power plant in the US deserts. Such a power plant could provide enough electricity to power around 100000 households (www.enviromission.com).
In October 2010 a so-called Solar Heated Wind Updraft Tower Power System became operational in the Wuhai desert, Inner Mongolia (China). It is a medium size power plant with a 53 m tall tower and a collector area of 6300 m^2. There are 5 turbines, each one having a capacity of 40 kW (Wei&Wu, 2012). In October 2010 the generating electricity system was combined to the grid and since then monitoring devices have been controlling the thermodynamic behaviour. Some pictures of the power plant, taken during a visit in October 2012, are reported in the following (Figure 1.7, Figure 1.8).

Figure 1.7 Solar Heated Wind Updraft Tower Power in Wuhai desert, Inner Mongolia (China). Visit to the prototype in October 2012, during the 3rd Int. Conf. on Solar Updraft Tower Power Technology.

a) *b)* *c)*

Figure 1.8 Solar Heated Wind Updraft Tower Power in Wuhai desert, Inner Mongolia (China). a) View of the tower under the glass collector, b) Tower, c) Turbine

1.3 Production of energy

The thermo- and fluid-dynamic behaviour of the power plant and the efficiency of energy production are crucial aspects for the development of the technology. However, they are not addressed in this work and only a simplified approach – resulting from documentation in literature – is presented now. For further details, the first wide studies of the multi-physics of solar updraft power plants can be found in Weinrebe (2000) and Bernades (2004). Then, Pretorius (2007) presents another milestone work. Recent studies are presented in Krätzig (2012a,b).

A simple theory to understand the mechanism of SUPPs is outlined in Schlaich (1995) and briefly addressed here. According to that, the efficiency of the power plant is the product of the individual component efficiencies, i.e. the collector roof, the solar tower and the turbines:

$$\eta = \eta_{coll} * \eta_{c} * \eta_{turb} \tag{1.1}$$

The efficiency of the collector (η_{coll}) describes the effectiveness with which solar radiation is converted into heat. The efficiency of the chimney (η_{c}) describes the effectiveness with which the quantity of heat delivered by the collector is converted into flow energy. η_{turb} is the efficiency of the wind turbines.

The collector

The collector converts solar radiation G (W/m^2) on the collector surface A_{coll} (m^2) into heat increase in the collector airflow $\dot{Q}$ (W). Thus, the efficiency of the collector is defined by the ratio:

$$\eta_{coll} = \frac{\dot{Q}}{A_{coll} * G} \tag{1.2}$$

In recent publications, Krätzig (2012a,b) applies one-dimensional flow-tube theory and prosecutes a mass of air on its way through the collector, the turbines and the chimney. The efficiency of the collector is estimated successively and iteratively for each one-dimensional collector element with a characteristic finite volume of air. The thermo-fluidmechanics in the collector is described by fluid equations (conservation of mass, conservation of momentum and Bernoulli's energy equation to connect the ambient atmosphere around the plant at the collector rim with its interior) and thermodynamic conditions (conservation of energy). Fluid equations and thermodynamic conditions are coupled by the equation of state of air, as an ideal gas.
The heat output $\dot{Q}$ under steady conditions is expressed as the product of the mass flow rate $\dot{m}$ (kg/s), the specific heat capacity of the air $C_{p,air}$ (J/kgK) and the temperature difference between the collector inflow and outflow (a typical value is $\Delta T \approx 30°K$):

$$\dot{Q} = \dot{m} C_{p,air} \Delta T \tag{1.3}$$

According to Pretorius (2007) the efficiency of the collector η_{coll} can be approximated by the following interpolation relation, in which the diameter of the collector D_{coll} is measured in km:

$$\eta_{coll} = 0.680 * \left(1 - 0.229 \sqrt{D_{coll} - 2}\right) \tag{1.4}$$

In order to model the physical processes of transformation of solar radiation G into heat increase ΔT of the air flux, the specific design of the collector comes into play. In

fact, the manifold exchanges of convective and radiation heat power that exist in the different components of the collector – single or double glass panels, air flow, water heat storage or soil absorber – must be considered in the heat power balance conditions (Krätzig, 2012a,b).

The chimney

The chimney converts the heat flow $\dot{Q}$ produced by the collector into kinetic energy.
The pressure difference Δp_{tot} between a column of cold air outside and a column of hot air inside the chimney is the driving force that causes air to flow through the Solar Updraft Power Plant.

$$\Delta p_{tot} = g \int_0^H \{\rho_a(z) - \rho_c(z)\} dz \tag{1.5}$$

$\rho_a(z)$ and $\rho_c(z)$ stand for the height-depending mass density (kg/m^3) of the air outside and inside the chimney, while g is the gravitational acceleration (m/s^2).
With the barometric pressure dependence from height, air as an ideal gas and ΔT constant over h, the pressure difference can be evaluated by solving analytically equation (1.5) over the tower height:

$$\Delta p_{tot} = g \rho_{coll} H \frac{\Delta T}{T_0} \tag{1.6}$$

being ρ_{coll} the density of air at temperature $T_0+\Delta T$ at collector outflow and T_0 the ambient temperature at ground level.
The pressure difference can be divided into a static and a dynamic component (neglecting friction losses):

$$\Delta p_{tot} = \Delta p_s + \Delta p_d \tag{1.7}$$

Such a division is due to the energy taken by the turbines: the static pressure difference drops at the turbines, while the dynamic component describes the kinetic energy of the airflow. If the turbines are left out (Δp_s=0), the maximum flow speed $V_{c,max}$ is achieved and the whole pressure difference is used to accelerate the air.

From Bernoulli's equation we calculate the maximum air velocity at the chimney's entrance:

$$V_{c,\max} = \sqrt{2gH\frac{\Delta T}{T_0}} \tag{1.8}$$

The whole pressure difference is then converted into kinetic energy. Therefore, the total power contained in the flow is:

$$P_{tot} = \Delta p_{tot}\frac{\overset{\bullet}{m}}{\rho} = \Delta p_{tot} V_{c,\max} A_c = \frac{1}{2}\overset{\bullet}{m} V_{c,\max}^2 \tag{1.9}$$

$V_{c,max}$ and A_c are the maximum flow speed and the cross-section of the chimney, respectively.
The efficiency of the chimney can be calculated by combining equations (1.3), (1.8), (1.9):

$$\eta_c = \frac{P_{tot}}{\overset{\bullet}{Q}} = \frac{gH}{C_{p,air}T_0} \tag{1.10}$$

All of that is a simplified representation, but it highlights that the efficiency of the chimney is fundamentally dependent on its height. Pretorius (2007) also proposes an approximated expression to consider the influence of the mean chimney diameter D.

The turbines

The turbines at the base of the chimney convert free convection flow into rotational energy. The pressure drop at the turbines can be expressed, in a first approximation, by the Bernoulli equation:

$$\Delta p_s = \Delta p_{tot} - \frac{1}{2}\rho_c V_c^2 \tag{1.11}$$

being ρ_c and V_c the air density and the flow speed in the chimney, respectively.
Thus, the theoretically useful power at the turbines becomes, in analogy to equation (1.9):

$$P_{tot} = \Delta p_s \frac{\dot{m}}{\rho} = \Delta p_s V_c A_c = \frac{1}{2} \dot{m} V_c^2 \tag{1.12}$$

By introducing η_{turb} for the turbine efficiency and the pressure withdrawal factor k_{pw} (so that $\Delta p_s = k_{pw} \Delta p_{tot}$)), the effective electrical power generated by the power plant can be finally expressed as:

$$P_{el} = k_{pw} \eta_{turb} \eta_{coll} \eta_c A_{coll} G \tag{1.13}$$

The power is maximized if the pressure drop $\Delta p_s = k_{pw} \Delta p_{tot}$ is about two thirds of the total pressure difference available, i.e $k_{pw} = 2/3$ (Schlaich, 1995). By substitution, it results:

$$P_{el} = \frac{2}{3} \eta_{turb} \eta_{coll} \frac{gH}{C_{p,air} T_0} A_{coll} G \tag{1.14}$$

The electrical output of the Solar Updraft Power Plant is then proportional to the product HA_{coll}, i.e. to the volume included within the chimney height and the collector area, as it was stated in section 1.1. Further detailed and updated studies can be found in Proc. SUTPT 2012.

Electric power and electricity costs

Despite the high initial cost of the SUPPs, the estimated leveled electricity costs LECs (due to IEA-guidelines) of the harvested energy are very low.

Krätzig (2012b) estimates a maximum electric power of 75 MW for a power plant with a 750 m tall chimney and 3500 m collector diameter, by assuming solar radiation G = 2.2 MWh/m^2. If the capacity factor (i.e. full load hours/24*365 hours in one year) is considered about 34%, - it means that the full load hours in one year are around 3000 - then the total annual energy harvest is around 75/0.34 = 220 GWh/a. The same paper provides an estimation of investment costs (around 340 M€, 60% of which due to the collector, 20% due to the chimney and 15% due to the turbines, plus extra costs). By considering a depreciation period of 33 years, it results in LECs equal to 9.9 €cent/kWh.

A similar value of LECs also resulted in other previous studies (Bergermann&Weinrebe, 2010). They estimated for a 200MW Solar Updraft Tower a total investment of 750 M€ and an average yearly production for a North African location of 650 GWh. It resulted, by assuming a depreciation period of 30 years, in LECs equal to 10.3 €cent/kWh.
Further studies about economic aspects can be found in (Breuer&Hüwe, 2010).

1.4 Main components of the power plant

1.4.1 The tower

Solar Updraft Towers (SUTs) are slender and extremely thin shells, usually made of reinforced concrete. In Europe, two main German schools are leading the structural design of Solar Updraft Towers, headed by J. Schlaich and W.B. Krätzig, respectively. J. Schlaich proposes tubes of cylindrical shape, usually stiffened along the height by spoke wheels. Various alternatives and non-linear structural analyses are reported in (Goldack, 2004, 2011). A double-wall tower is also presented in (Goldack, 2004). Two examples are shown in Figure 1.9 and Figure 1.10.

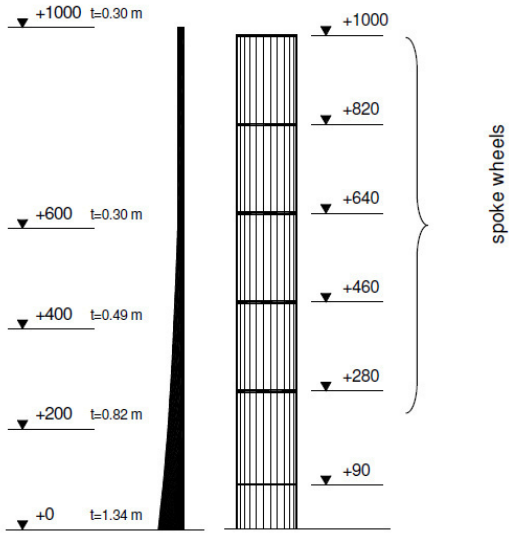

Figure 1.9 1-km tower (Goldack, 2004, 2011)

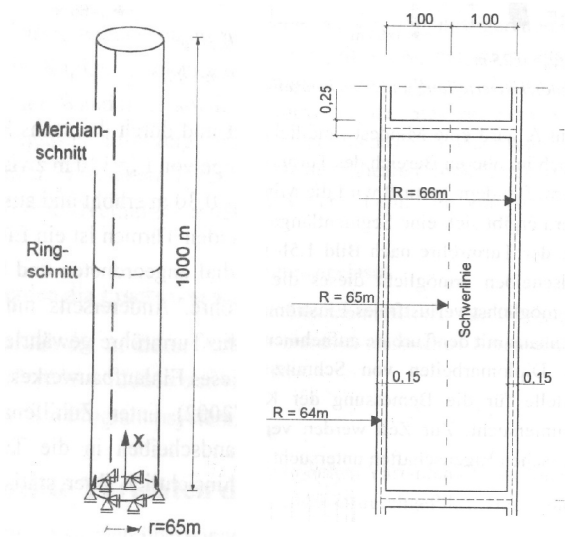

Figure 1.10 Double-wall tower (Goldack, 2004)

W.B. Krätzig transfers insights from designs of natural draft cooling towers' projects to solar chimneys. Figure 1.11 gives an overview over these attempts, demonstrating the way from cooling towers to chimneys of SUPPs up to an elevation of 1500 m (Krätzig et al., 2008-2009a,b).

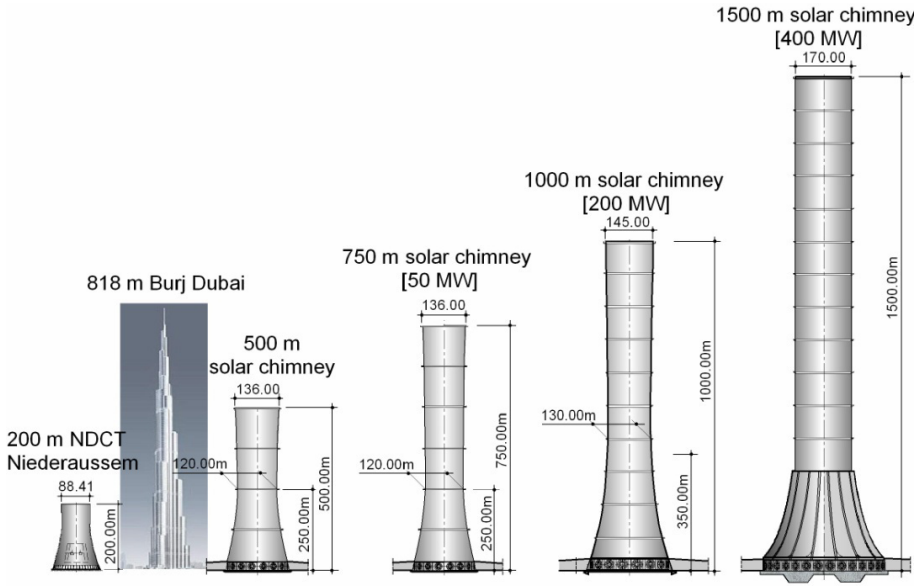

Figure 1.11 From cooling towers to chimneys of Solar Updraft Power Plants (Krätzig et al., 2008-2009a,b)

The distinctive feature is that the lower part of the tower turns into a hyperboloid. Thanks to the use of a double curvature surface, the structure applies the benefits of shape strengthening. Two recent pre-designs of a 1000 m high reinforced concrete solar tower are shown in Figure 1.12 and Figure 1.13 (Krätzig et al., 2008-2009a,b; Harte et al., 2010). With a collector size of 6000 m of diameter they shall produce a peak power of 200 MW_p (annual work of 600 GWh). In Figure 1.12, shortly above the throat at 400 m of height, the shell diameter is 130 m wide, while at the upper ring it is 145 m. Below 400 m the tower shell widens in strength-optimized hyperbolic shape up to a foot-diameter of 260 m. The wall thickness of high-performance reinforced concrete (C70/85) varies from 0.25 m to 0.65 m. In addition to the upper edge member, nine intermediate reinforced concrete ring-stiffeners are applied, fixed on the outer shell face. 16 turbo-generators deliver the mentioned plant capacity, see (Backström et al, 2008). In Figure 1.13 the upper part of the tower has a constant diameter of 150 m and the maximum shell thickness at the base is 0.60 m. This one drawn in Figure 1.13 is the reference structure which is always considered in this work.

From the structural viewpoint it is important to construct the solar tower as thin as possible. This can be achieved by using high-strength concrete and/or by installing stiffening rings along the chimney height and on top. Stiffening rings can be realized in several ways, e.g. classical reinforced concrete beams (Figure 1.14), composite steel-concrete, spoken wheels with carbon fiber strings (Figure 1.15). In order not to reduce the efficiency of production, the interference between stiffening rings and

internal efflux in the chimney has to be minimized. For this reason, it is preferable that stiffening rings are fixed on the outer surface.

Firstly, the intermediate stiffeners enhance a beam-like distribution of the meridional forces under wind loading. The second important contribution of the rings is the increase in the stability safety by localization of the buckling modes. For tower designs without ring-stiffeners one would recognize that instability modes dominate the entire shell, so that the concrete quality for this alternative had to be increased to a high performance reinforced concrete (e.g. C90/105), (Krätzig et al., 2008-2009a,b). Moreover, the vulnerability to vortex shedding would be strongly increased if the shell-like behaviour predominated at the first eigenmode.

Provided a very good soil, the foundation of 1 km tower may only consist of a reinforced concrete circular ring beam (Krätzig et al., 2008-2009a,b).

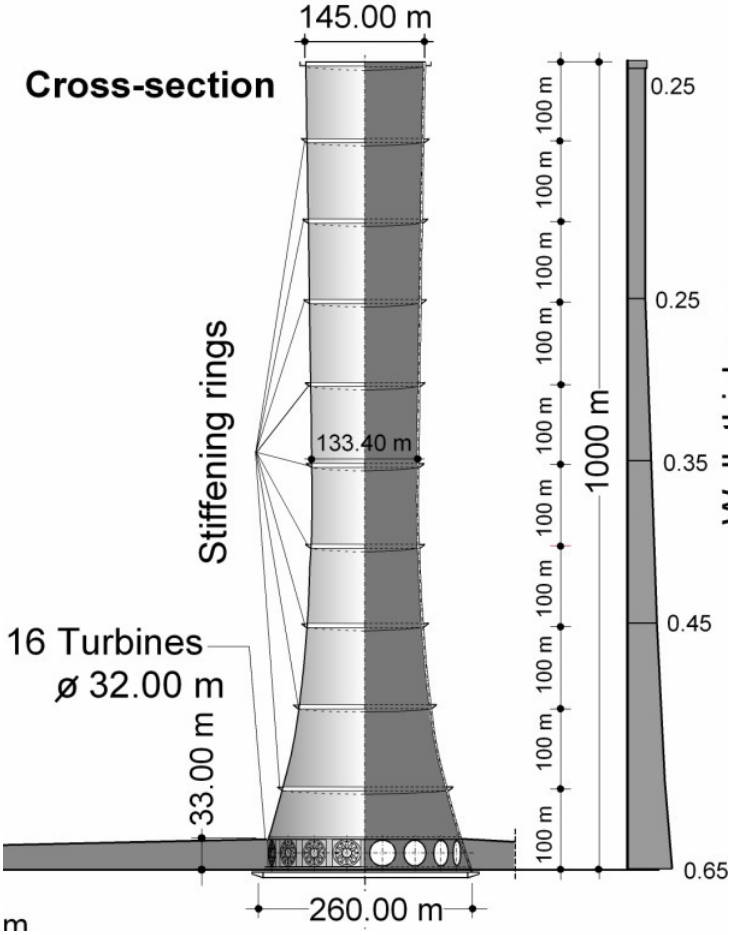

Figure 1.12 Example n.1 of 1-km tall solar tower (Krätzig et al., 2008-2009a,b; Harte et al. 2010)

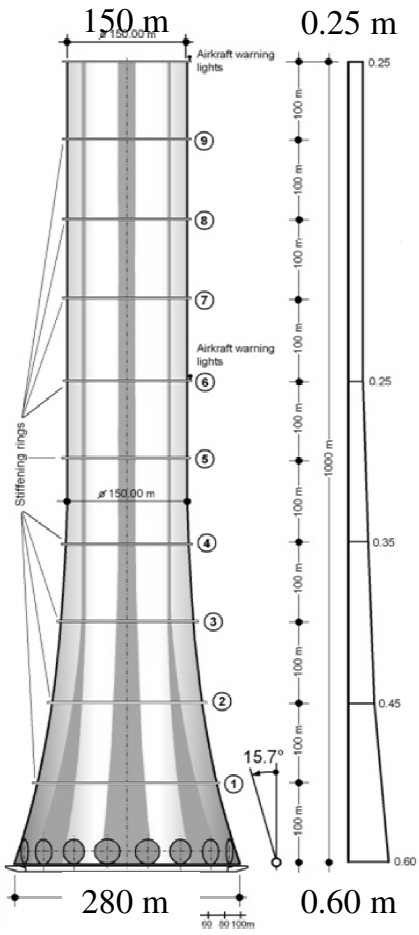

Figure 1.13 Example n.2 of 1-km tall solar tower (Krätzig et al., 2008-2009a,b; Harte et al. 2010)

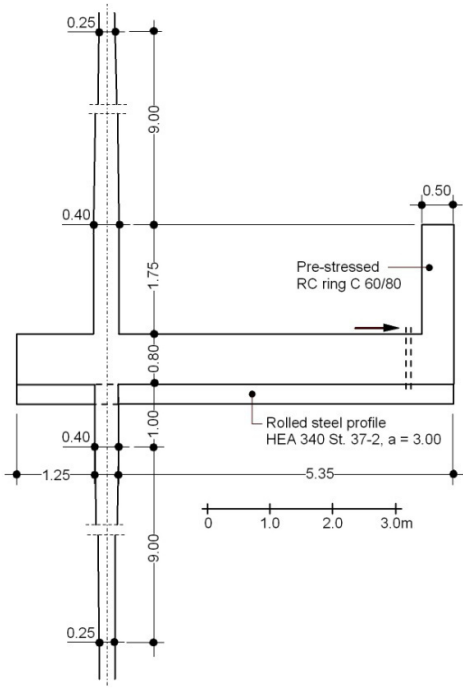

Figure 1.14 Reinforced concrete stiffening ring (Krätzig et al., 2008-2009a,b)

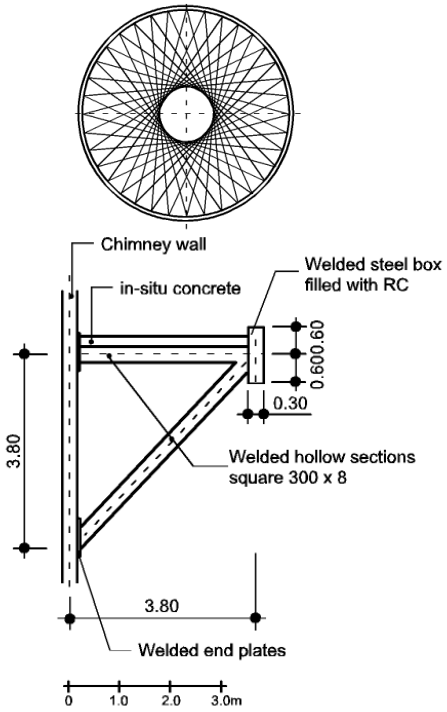

Figure 1.15 Spoke wheels with carbon fiber strings (Krätzig et al., 2008-2009a,b)

1.4.2 **The collector**

The collector area is not investigated within this work. However, the collector is one of the main components of the power plant. In fact, as previously mentioned, the power output of Solar Updraft Towers is proportional to the collector area (1.14). The diameter of the collector ranges from 1 up to 7 km, depending on the required energy output, it is usually made of glass and it could also take the secondary function of being a greenhouse for agricultural purposes. Its cost is a high percentage (between 40% and 60%) of the entire power plant, as reported in several publications (e.g. Krätzig , 2012b; Bergermann&Weinrebe, 2010). Thus, the collector plays a key role and the performances of the SUPP, in terms of energy production, can be significantly increased by improving the collector glass quality. In particular, the optical glass quality is of the greatest importance. The transmittance and absorptivity of glass depend on the solar radiation incident angle, the refractive index of the glass, the thickness of the glass and its extinction coefficient. The latter determines the amount of radiation absorbed and consequently transmitted by the medium (Pretorius, 2007). Moreover, a better quality of the glass implies a better transparency, allowing more solar radiation to penetrate it.

Several studies and on-going researches about the collector can be found in literature. For example, numerical simulations are performed in (Pretorius, 2007), referring to a SUPP located in South Africa, with a 5000 m collector diameter and a 1000 m high, 210 m diameter chimney. These simulations show that through the modification of the collector roof reflectance, collector roof emissivity, ground surface absorptivity and ground surface emissivity, major improvements on plant performance are possible. An improved plant performance can also be reached by introducing thermal insulation and double glazing of the collector roof. The better is the insulation of the warm collector air from the environment, the smaller are the heat losses through the roof. It is also predicted a notable sensitivity to the ground surface absorptivity value.
Techniques to control the power output of a SUPP according to specific demand patterns are investigated in (Pretorius, 2007). Without any control, SUPPs deliver electricity simultaneously to sun radiation and are designed neither for base load power generation nor for peak load. The introduction of a secondary collector roof beneath the main one is a strategy proposed by Pretorius to regulate the air-flow, and thus the energy production, according to specific demand patterns. Another strategy to control the power production of SUPPs is the incorporation of water tanks under the collector roof, so that the energy (heat) storage capability increases significantly thanks to the high specific heat capacity of water. In this way, the production during the day-time is lower, but the night-time production is much higher.
Recent studies about heat storage and heat transfer have been presented at the International conference SUTPT 2012 (e.g. Bernardes (2012) and Fasel (2012)).

1.4.3 **The turbines**

Milestones studies regarding the layout of the turbines of solar updraft towers belong to the University of Stellenbosch (Backström&Fluri, 2006; Fluri, 2008; Fluri&Backström, 2008; Backström&Fluri, 2010).
The two typical solar tower configurations are one with vertical axis (used in a single turbine layout) and one with horizontal axis (used in multiple turbine layout). Backström&Fluri (2010) explain that the vertical axis layout with horizontal entrance is favoured for layouts where there is one turbine per chimney, while the horizontal layout for many turbines per chimney. In Fluri (2008) it is stated that many smaller generators replacing a large one weigh and cost less than a huge one. Fluri investigated the optimum number of turbines for solar chimney power plants of various output. He found that for large plans with nominal power of 200 MW the optimal number of

turbines is about 30, and the turbine diameter is about 30 m. Each turbine will then have a rating of about 6.7 MW.
The turbine layout is not considered in this work. However, the reference structure of this Thesis, depicted in Figure 1.13 presents 16 turbines of 32 m in diameter.

1.5 Aim of the research

The dissertation investigates the Aeolian risk scenario on ultra-high structures, like solar updraft towers. For such structures, the wind action represents the main natural hazard.
At first, the dissertation aims to revise the knowledge about the nature of strong winds in the atmospheric boundary layer. The usual wind engineering applications are limited to the lowest 200-300 m of the atmosphere, where codified wind profiles can be applied. The coupling between wind engineering and meteorology allows to investigate higher levels. The problem is addressed in the thesis on theoretical bases, because experimental data at large heights in strong winds are, so far, inexistent. Several issues still remain unsolved and their uncertainty increases the structural risk of ultra-high towers. However, this should not prevent the design, provided that the vulnerability of the structure to the wind action is low.
The structural vulnerability of solar towers to the wind action is especially addressed in the dissertation. In fact, so far it was known that stiffening rings applied along the height of the tower reduce the vulnerability of the structure, because they enhance a beam-like behaviour. However, their effect on the load had never been investigated before. Moreover, no load model is so far available to the designer to calculate the structural response of a solar updraft tower to a stochastic wind loading process. Without that, the actual damage of such a structure due to the wind action could not be really estimated.
Thus, the main purpose of this research is to investigate – by means of wind tunnel experiments – the aerodynamics of the flow around circular cylinders, like solar towers. Beside the traditional case of study, i.e. a circular cylinder with a free-end (which is addressed in literature but not in all its aspects) the dissertation also investigates the effect of rings along the height of the tower. This case is not treated in literature. The dissertation aims at investigating the new phenomenon created by spanwise rings, both from the fluid dynamic point of view – by means of wind tunnel experiments and numerical simulations – and from the structural point of view.

The experimental investigation is performed in two wind tunnels, at WiSt Ruhr-University Bochum and at CRIACIV University of Florence. The comparative study aims to cross-check results. In view of that, numerical simulations represent a further support. However, the wind pressures depend on atmospheric boundary layer characteristics. Since the boundary layers in two different wind tunnels are necessarily different, the experiments also aim to investigate such a dependency. So, as a further result of this work, the designer will benefit of a quasi-static stochastic load model which is not referred to a pre-defined boundary layer, but it can be generalized to any atmospheric boundary layer flow. This tool allows to evaluate the structural damage even in the vicinity of the stiffening rings, where the shell-like behaviour predominates and no load model was available before.

The tower structure which is used as reference in the dissertation is the one in Figure 1.13. The height is 1-km, the diameter at the base is 280 m and at the top it is 150 m. However, the wind tunnel model has a simpler and more general shape. It is a circular cylinder with aspect ratio H/D = 1000/150 = 6.7.

Chapter 2. **Risk scenario for SUPPs technology**

This chapter describes the risk scenario of the apparently most economic and sustainable technology for renewable energy harvesting, with focus on the Aeolian risk. The theory of the atmospheric boundary layer at large heights – resulting from coupling wind engineering with boundary layer meteorology – is presented as the basis for a deeper knowledge of the natural hazard. Moreover, so far it is known that the structural vulnerability of the tower to the wind action can be reduced by introducing stiffening rings along the height.

2.1 **Aeolian risk**

Many studies around the world (SCPT, 2010; SUTPT, 2012) proved that Solar Updraft Power Plants would be the most economic technology for renewable energy harvesting in the world, as reported in section 1.3. The leveled electricity costs of the energy (according to the definition in the IEA-guidelines) would be of a few €cent/kWh, considerably lower than those for other competitive renewable energy concepts. So, why have big power plants not come to realization, yet? It is not only a matter of the high initial cost, because it would be retrieved after the amortization period, including depreciation. In fact, SUPPs are considered a highly risky technology. The high risk concerns especially two main aspects: the production of energy and the structural feasibility. Some projects stopped before being completed because it was realized that the production of energy of the power plant would have resulted lower than expectations, for which investors were gained. The structural aspect is another challenge, since 1 km tower would be the highest structure in the world.
The present work focuses on the structural aspect; the wind action on the tower is selected among all natural hazards. Thus, the focus is on the Aeolian risk scenario, which is first introduced in the next section within a general framework. In particular, the following issues are discussed in the dissertation:

NATURAL HAZARD

The state of knowledge of the nature of wind at high altitudes results from coupling boundary layer meteorology with wind engineering. Theoretical models like the Harris and Deaves (H&D) one (Harris&Deaves, 1980) describe the mean wind profile, the turbulence intensity and the integral length scale of turbulence in strong wind

conditions up to the boundary layer height, on the basis of order of magnitude analyses of the equations of motion. The Coriolis force is included. However, a further question is whether such mid-latitudes models could be applied at small latitudes, where the Coriolis force becomes smaller and smaller in the geostrophic balance. Moreover, to which extent can full-scale measurements at large heights (e.g. 1 km height) be used to study the turbulent properties of wind, for engineering purposes? These issues are addressed in section 2.3. Tropical cyclones and tornadoes are only mentioned but not included in this work.
Wind tunnel experiments performed in different boundary layers (and different wind tunnels) allowed to study the effect of certain boundary layer properties on wind forces and pressures. A simplified model of wind pressures on the tower shell, with regard to the turbulent properties of the incoming flow, is proposed in Chapter 7. It can be applied by the designer in any boundary layer flow to calculate the quasi-static response of the tower (resonance not included).

EXPOSURE

The tower is considered exposed to strong wind conditions (exposure factor E = 1).

VULNERABILITY

The main part of the dissertation studies the effect of stiffening rings applied along the height of the tower, like those reported in Figure 1.14 and Figure 1.15. They were originally introduced in the design in order to reduce the vulnerability of the structure, as explained in section 2.4, but their effect on the flow had never been investigated before. The thesis discovers and proves that this strategy for the reduction of structural vulnerability might induce an even more severe load condition, if improperly used.

2.2 Risk management framework

The risk scenario of the Solar Updraft Power Plants Technology can be described within the general approach of the risk management framework. The latter is outlined as a unified methodology throughout different disciplines in Pliefke (2010).

The risk management framework is organized in three main steps (see Figure 2.1), that are risk identification, risk assessment and risk treatment. They are performed sequentially and accompanied by a risk review step and a continuous risk monitoring.

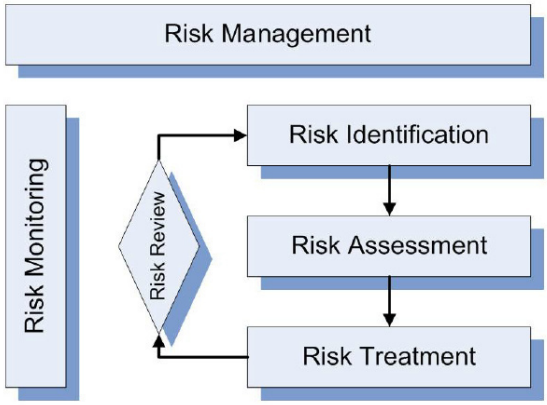

Figure 2.1 The general risk management framework (Pliefke, 2010)

As outlined in Pliefke (2010), the risk identification phase consists in the definition of the system under analysis and of the hazards that could endanger it. In the present work, the system is the solar tower and the natural hazard under investigation is the wind action.

The risk assessment phase is divided in two sub-steps (Figure 2.2): the risk analysis and the risk evaluation. The risk analysis (Figure 2.3) consists in a quantification of the risk. To do that, the hazard must be defined, for a certain return period, in term of its intensity and frequency parameters. Then, for each element at risk (EaR) of the system, i.e. for each element with a non-zero exposure to the hazard, the impact of the hazard is converted into hazard load. Depending on the structural response of the element at risk to the hazard load, the damage can be identified. The relation between the hazard load and the resulting damage is the structural vulnerability. It indicates "the degree of physical susceptibility towards the impact of the hazard". The expected damage per year can be interpreted as the structural risk. By definition, the structural risk is "the product of the annual probability of occurrence of damage multiplied by the potential damage that goes in line with it". Then, direct and indirect consequences, both tangible and intangible, are estimated in order to calculate the total risk, i.e. the expected loss per year, which is "the product of the annual probability of occurrence of the loss and the loss that goes in line with it". Tangible consequences are measured in monetary value. Intangible consequences must be converted in monetary values, otherwise no comparison of risks is possible. After that, the risk evaluation sub-step aims to find adequate risk measures, so that the risk under investigation can be compared to other risks for the system.

The last phase in Figure 2.1, that is the risk treatment, creates a rational basis to handle the risk and, if necessary, reduce it by risk mitigation initiatives. Then, for those risks that have already run through the whole process at least once, a risk review process can be performed.

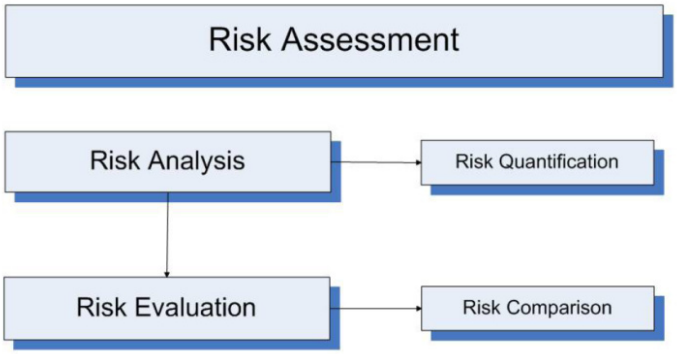

Figure 2.2 The risk assessment phase (Pliefke, 2010)

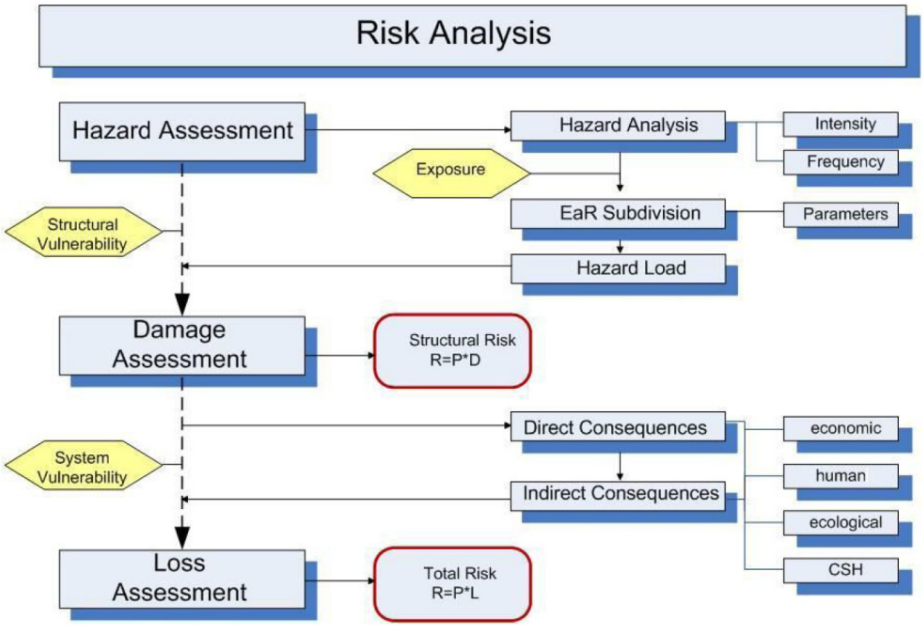

Figure 2.3 The risk analysis (Pliefke, 2010)

The risk management framework proposed by Pliefke is consistent with other definitions of risk in literature. In particular, Augusti et al., (2001) define the damage risk as "the risk associated with physical damage to constructed facilities". The probability of a negative consequence caused by a potentially dangerous event is "the product of three factors, namely: [1)] hazard, i.e. the probability of occurrence of a dangerous event (the action); [2)] exposition, i.e. the probability that the action finds something that can be damaged; [3)] vulnerability, i.e. the (conditional) probability that the facility is damaged when hit by the dangerous action." The damage is associated to its consequences ("losses"). The latter can be considered as a measure of the damage itself, so that the three-factor formulation yields directly the risk as "expected cost of damage". Alternatively, the "expected cost of damage" can be split up into the product of the "probability of damage" times the "cost of damage". In this case, the cost of damage is the fourth factor to be included in the probabilistic definition of risk.

2.3 Natural hazard – the wind action

Solar Towers are subjected to loads and other actions that are typical for high reinforced concrete towers:

- dead load of the shell wall, the ring beams, the turbine houses, and the foundation ring;
- wind loading acting both on the external and the internal surfaces of the shell
- temperature effects, operational ones from the action of the heated air, axisymmetrical ones due to ambient air temperature, non-axisymmetrical ones due to solar irradiation on the tower shell;
- seismic action if the location of the Solar Updraft Power Plant exhibits sufficiently important seismicity;
- shrinkage effects;
- pre-stressing if applicable;
- construction loads, e.g. anchor forces from pre-stressed guys of the central crane;
- differential soil settlements of external origin.

Wind and seismic activity are the main natural hazards to be considered in the tower design. However, the very high first natural period of the tower (beam-like bending mode, like a soft cantilever), makes it isolated against strong earthquake excitations. Therefore, even in case of seismic hazard, the vulnerability of the structure to earthquake loading is not high. The seismic risk is thus neglected in this work. Instead, the main risk in the solar tower design is due to the wind action.

The wind hazard for strong winds in “well-behaved” wind climates (i.e. excluding tropical cyclones and tornadoes) is related to the design wind velocity. This is the 10-min-average velocity that has a 2% yearly probability of exceedance, which roughly corresponds to a 50-year-return period (Eurocode1). Tropical cyclones and tornadoes are not covered in this dissertation (they are only mentioned in section 2.3.4), as well as occurrence of low-level jets in the deserts.

The height of solar updraft towers (up to 1500m) exceeds by far the main definition domain of up to 300 m for established and codified wind profiles and wind load models. In this domain, the concept of the turbulent Prandtl layer with constant shear is a useful approximation. Above the Prandtl layer, in the Ekman layer, the shear turbulence decreases while the Coriolis force increases and tends to align the flow in the direction of the isobars according to the Ekman spiral.

The knowledge of the nature of the wind is a pre-requisite for investigating the wind load on solar towers. However, experimental data are scarce at large heights, and accurate measurements of wind turbulence are currently not available above 300 m. This section addresses the state of knowledge of the structure of strong winds at high altitudes and to which extent it can be enhanced by means of field measurements. The modelling of the wind action with regard to turbulent properties of the flow (Chapter 7) by means of wind tunnel experiments in different boundary layer flows is the way which is proposed in this work to approach the open problem concerning the nature of wind at large heights.

2.3.1 The structure of strong winds in the atmospheric boundary layer

Five equations form the foundation of boundary layer meteorology (Stull, 1988): [1)] equation of state (ideal gas law), [2)] conservation of mass (continuity equation), [3)] conservation of momentum (Newton's second law), [4)] conservation of moisture, [5)] conservation of heat (first law of thermodynamics). In addition, there are equations for conservation of scalar quantities, e.g. a tracer in the atmosphere.

In strong winds, it can be assumed that the ambient temperature gradient is adiabatic (neutrally stable atmosphere), so that only the mechanical stirring and not the convective action of buoyancy forces will generate turbulence. Essentially, the conservation of momentum and the continuity equation govern the motion of strong atmospheric winds. The latter leads to the incompressibility approximation if typical velocity and length scales of the boundary layer are used. In a rotating Cartesian frame of reference the former equation is (Stull, 1988):

$$\underbrace{\frac{\partial U_i}{\partial t}}_{\text{I}} + \underbrace{U_j \frac{\partial U_i}{\partial x_j}}_{\text{II}} = \underbrace{-\delta_{i3} g}_{\text{III}} + \underbrace{f_c \varepsilon_{ij3} U_j}_{\text{IV}} \underbrace{- \frac{1}{\rho} \frac{\partial p}{\partial x_i}}_{\text{V}} + \underbrace{\frac{1}{\rho} \frac{\partial \tau_{ij}}{\partial x_j}}_{\text{VI}} \qquad (2.1)$$

where i,j = 1,2,3 and ε_{ij3} = +1 if ij3 = 123 and = -1 if ij3 = 213; ε_{ij3} = 0 if i = j (alternating unit tensor) and δ_{i3} = +1 if i = 3, otherwise it is 0 (Kronecker delta). The terms on the left-hand side represent the time rate of change of the wind velocity (i.e. acceleration) following a moving fluid element: the first contribution (term I) is the time rate of change at a fixed point (local derivative), while the second term (term II, advection) is the time rate of change due to the movement of the fluid element from one location to another in a flow field where the flow properties are spatially different. The terms on the right-hand side represent the sum of forces (per unit mass) acting on

a fluid particle. They are body forces (term III, due to gravity and acting only vertically), Coriolis force (term IV, an apparent force due to the earth rotation, f_c is the Coriolis parameter), pressure-gradient forces (term V) and viscous forces (terms VI).
To a close approximation, air in the atmosphere behaves like a Newtonian fluid (viscous stresses are proportional to the velocity gradients), so that, by assuming incompressibility, the term VI reduces to:

$$\text{Term VI} = \frac{1}{\rho}\frac{\partial \tau_{ij}}{\partial x_j} \rightarrow \nu \frac{\partial^2 U_i}{\partial x_j^2} \tag{2.2}$$

$$\text{being: } \nu = \frac{\mu}{\rho} \text{ the kinematic viscosity and } \tau_{ij} = \mu\left(\frac{\partial U_i}{\partial x_j} + \frac{\partial U_j}{\partial x_i}\right) \tag{2.3}$$

The horizontal pressure gradient term (V) can be expressed by using the definition of geostrophic wind:

$$f_c U_g = -\frac{1}{\rho}\frac{\partial p}{\partial y} \quad \text{and} \quad f_c V_g = +\frac{1}{\rho}\frac{\partial p}{\partial x} \tag{2.4}$$

So that the horizontal equations of motion can be written as:

$$\frac{dU}{dt} = -f_c\left(V_g - V\right) + \nu\frac{\partial^2 U}{\partial x_j^2} \tag{2.5}$$

I+II IV+V VI

$$\frac{dV}{dt} = +f_c\left(U_g - U\right) + \nu\frac{\partial^2 V}{\partial x_j^2} \tag{2.6}$$

I+II IV+V VI

where the terms IV+V are sometimes called the geostrophic departure terms because they are zero when the actual winds are geostrophic.

Then, the wind velocity can be expanded into mean and fluctuating components. It is remarkable that, due to the non-linearity of the equations, unknown terms arise even in the equations of the mean fluid motion (equations (2.7)). They are the Reynolds stresses. Physically, this implication means that turbulence must be considered in making forecasts in the turbulent boundary layer, even if only mean quantities are of interest. The following forecast equation for mean wind is formally very similar to the basic conservation equation (2.1) except for the addition of the turbulence term at the end (VII):

$$\underbrace{\frac{\partial \overline{U_i}}{\partial t}}_{\text{I}} + \underbrace{\overline{U_j}\frac{\partial \overline{U_i}}{\partial x_j}}_{\text{II}} = \underbrace{-\delta_{i3} g}_{\text{III}} + \underbrace{f_c \varepsilon_{ij3} \overline{U_j}}_{\text{IV}} \underbrace{- \frac{1}{\rho}\frac{\partial \overline{p}}{\partial x_i}}_{\text{V}} + \underbrace{\nu \frac{\partial^2 \overline{U_i}}{\partial x_j^2}}_{\text{VI}} \underbrace{- \frac{\partial \left(\overline{u_i' u_j'} \right)}{\partial x_j}}_{\text{VII}} \qquad (2.7)$$

In order to solve the problem, the unknown Reynolds stresses must be somehow specified (closure problem).

Mean wind profile

Some simplifying assumptions are introduced in meteorology, in order to develop analytical expressions of the mean wind profile throughout the whole depth of the boundary layer, including the Coriolis force (Stull, 1988):

- steady state ($\rightarrow \partial(\overline{\ })/\partial t = 0$, i.e. no time-dependence);
- horizontal homogeneous flow, as it happens in large-scale storms, on a horizontal site of uniform roughness over a sufficiently large fetch ($\rightarrow \partial(\overline{\ })/\partial x = 0, \partial(\overline{\ })/\partial y = 0$, i.e. no advection);
- barotropic flow, i.e. negligible horizontal density gradient ($\rightarrow$ constant geostrophic wind);
- geostrophic approximation ($\rightarrow$ the curvature of the isobars is negligible);
- no subsidence ($\rightarrow$ the mean vertical wind component is zero).

In these conditions, the equations of mean motion reduce to (Stull, 1988):

$$0 = f_c \overline{V} - \frac{1}{\rho}\frac{\partial p}{\partial x} + \frac{1}{\rho}\frac{\partial \tau_x}{\partial z} \qquad \rightarrow \qquad 0 = -f_c \left(\overline{V_g} - \overline{V} \right) + \frac{1}{\rho}\frac{\partial \tau_x}{\partial z} \qquad (2.8)$$

$$0 = -f_c \overline{U} - \frac{1}{\rho}\frac{\partial p}{\partial y} + \frac{1}{\rho}\frac{\partial \tau_y}{\partial z} \quad \rightarrow \quad 0 = +f_c\left(\overline{U_g} - \overline{U}\right) + \frac{1}{\rho}\frac{\partial \tau_y}{\partial z} \tag{2.9}$$

where τ_x and τ_y are the horizontal shear stresses, including both contributions from viscous forces and Reynolds stresses. $\overline{U}$ and $\overline{V}$ are the components of the mean wind. For convenience, it is chosen a reference system with the x-axis aligned with the direction of gradient wind G:

$$-\overline{V} f_c = +\frac{1}{\rho}\frac{\partial \tau_x}{\partial z} \tag{2.10}$$

$$f_c\left(\overline{U} - G\right) = \frac{1}{\rho}\frac{\partial \tau_y}{\partial z} \tag{2.11}$$

where:

$$G = \sqrt{U_g^2 + V_g^2} \tag{2.12}$$

The boundary conditions are:

$$z = 0 \quad \rightarrow \quad \overline{U} = \overline{V} = 0 \tag{2.13}$$

$$z \rightarrow \infty \ \rightarrow \ \overline{U} \rightarrow G\,,\ \overline{V} \rightarrow 0 \ \text{ and } \ \tau_x,\ \tau_y,\ \frac{\partial \tau_x}{\partial z},\ \frac{\partial \tau_y}{\partial z} \rightarrow 0 \tag{2.14}$$

Meteorologists have attempted to solve equations (2.8) and (2.9) by introducing phenomenological relations to describe the shear stresses τ_x and τ_y.
A well-known assumption (Schlichting, 1960) is that an eddy viscosity K and a mixing length L may be defined, so that (first-order local closure K-theory):

$$\frac{\tau_x}{\rho} = -K\frac{\partial \overline{U}}{\partial z} \ \text{ and } \ \frac{\tau_y}{\rho} = -K\frac{\partial \overline{V}}{\partial z} \tag{2.15}$$

where:

$$K(x,y,z) = L^2(x,y,z)\left[\left(\frac{\partial U}{\partial z}\right)^2 + \left(\frac{\partial V}{\partial z}\right)^2\right]^{1/2} \tag{2.16}$$

Either the eddy viscosity K or the mixing length L must be specified. An analytical solution of the equations (2.8) and (2.9) can be obtained under the assumption of a constant eddy viscosity (Ekman, 1905). That is the Ekman spiral model:

$$\overline{U}(z) = G\left[1 - e^{-\gamma_E z}\cos\left(\gamma_E z\right)\right] \tag{2.17}$$

$$\overline{V}(z) = G\left[e^{-\gamma_E z}\sin\left(\gamma_E z\right)\right] \tag{2.18}$$

where $\gamma_E = (f_c/2K)^{1/2}$, and $f_c = 2\Omega\sin\phi$ is the Coriolis parameter (ϕ = latitude, Ω = angular velocity of Earth rotation). The wind speed is geostrophic at height $z = \pi/\gamma_E$. This height is used as an estimate of the depth of the neutral boundary layer. Hence, the Ekman layer depth can be defined as $h = \pi/\gamma_E$.

A different type of approach, based on the asymptotic similarity theory, is developed in Csanady (1967). The boundary layer is divided in two regions: a surface layer and an outer layer. The theory is based on the attempt to express the profile of wind velocity as a function of height in non-dimensional form. This poses the problem of finding appropriate velocity and length scale parameters. It turns out that for the velocity, anywhere in the height range considered, the velocity scale parameter is the friction velocity u_*. In the case of the height scale, in the lower layer, close to the ground, the appropriate parameter is the roughness length z_0, while in the upper layer it is the gradient height h. The law of the wall describes the flow in the surface layer, while a velocity defect law applies in the outer layer.
The key to solve the problem lies in the assumption that a region of overlap exists, in which both laws are valid. It results in a logarithmic solution. Out of it, the gradient wind velocity can be calculated (Gill, 1968; Monin&Yaglom, 1971). It depends on two universal constants A and B:

$$G = \left[B^2 + \left(\ln \frac{u_*}{f_c z_0} - A \right)^2 \right]^{1/2} \frac{u_*}{k} \tag{2.19}$$

Several authors proposed values for A and B, as listed in Simiu&Scanlan (1996). It can be considered $0 < A < 2.8$ and $4.3 < B < 5.3$.

A similar approach, based on a modified version of the asymptotic similarity theory, was developed by Harris&Deaves (1980). The peculiar feature of the so-called H&D model is the closure assumption to solve the equations of motion (2.8) and (2.9): the shear stresses are assumed to decrease parabolically with height (equation (2.20)). Some justification for this assumption was found by the authors in full-scale data, but it is also justifiable on theoretical grounds, on the basis of an order of magnitude analysis between production, diffusion and dissipation of turbulent energy (Deaves, 1981).

$$\tau(z) = \rho u_*^2 \left(1 - \frac{z}{h} \right)^2 \tag{2.20}$$

This expression is adopted by the ESDU Data Items (ESDU 85020).
Accordingly, the velocity defect law is parabolic for a substantial part of the boundary layer, so that:

$$\overline{U}(z) = \frac{1}{k} u_* \left\{ \ln \frac{z}{z_0} + a_1 \frac{z}{h} + a_2 \left(\frac{z}{h} \right)^2 + a_3 \left(\frac{z}{h} \right)^3 + a_4 \left(\frac{z}{h} \right)^4 \right\} \tag{2.21}$$

where z_0 is the roughness length, h is the atmospheric boundary layer thickness, u_* is the friction velocity and k the Von Karman constant ($k = 0.4$). The coefficients a_i, i = 1, ..., 4 are universal constants whose values are determined theoretically, in terms of two experimental parameters: β and A. From fitting a number of good quality wind profiles, it resulted β = 6 and A = -1 (Harris&Deaves, 1980). So that:

$$a_1 = 2(\ln \beta - A) + \frac{1}{6} \approx 5.750 \quad a_2 = 1 - \frac{a_1}{2} = -1.875 \quad a_3 = -\frac{4}{3} \quad a_4 = \frac{1}{4} \tag{2.22}$$

The H&D model thus extends the log-law (which fits good near the surface) through the Ekman layer, in order to blend into the gradient wind velocity at the gradient height. Indeed, if compared to both the well-known logarithmic and power laws, the Harris and Deaves model is the only one which recognizes the top of the atmospheric boundary layer.

It is known that the boundary layer height (h) in neutral atmosphere is proportional to the ratio between the friction velocity and the Coriolis coefficient (Csanady, 1967). In the H&D model such proportionality is expressed by the coefficient 1/β:

$$h = \frac{1}{\beta}\frac{u_*}{f_c} \tag{2.23}$$

In order to give an idea of the boundary layer height, at a latitude $\phi = 30°$ it results $h \approx 4300$ m, being $z_0 = 0.05$ m, $V_b = 25$ m/s (at 10 m). Thus, the Deaves and Harris model has three scaling parameters: z0 and u* – inherited from the log-law model – and the additional length parameter, h, which is the atmospheric boundary layer height. It is a function of the wind speed, the surface roughness and also the latitude.
Then, by evaluating the H&D wind profile at z = h, the gradient wind speed is given by:

$$G = \frac{1}{k}u_*\left\{\ln\frac{u_*}{f_c z_0} - A\right\} \tag{2.24}$$

This expression is comparable with equation (2.19), but the universal constants have different values. The same letter A is used in expressions (2.19) and (2.24), because this is the traditional nomenclature reported in the literature on this topic. This should not create confusion. Finally, by using the closure assumption (2.20) and by applying the boundary conditions to the equations of motion, the H&D model derives the following relationship involving ϑ_0, the total (maximum) angle of turn of the wind throughout the boundary layer:

$$\frac{G\sin\vartheta_0}{u_*} = 2\beta = 12 \tag{2.25}$$

The model also suggests to use above the Prandtl layer a linear variation with height of the wind rotation angle. In fact, the variation of the wind angle would result from the solution of partial differential equations, but a linear approximation can be accepted.
In conclusion, relying on the closure assumption (2.20) – derived by an order-of-magnitude analysis – on the boundary conditions, on theoretical considerations and two constants (A and β) determined empirically, the H&D model gives a complete description of the mean flow in the atmospheric boundary layer (equation (2.21))[1]. However, this is valid at mid-latitudes, where a state of dynamic equilibrium establishes in strong wind conditions, so that the energy subtracted by the mean flow exactly balances that absorbed by the work done against surface friction and dissipated by the viscosity of air (Harris&Deaves, 1980). At tropical latitudes, strong winds are associated with large scale storms, but these may contain intense components of thermal origin. Moreover, the geostrophic assumption is more approximated as the Coriolis force becomes small. To which extent the H&D model is valid at small latitudes is addressed in section 2.3.3.

Standard deviation of the along-wind component σ_u

The H&D model also provides an analytical expression of the standard deviation σ_u of the along-wind component of turbulence at any height in the atmospheric boundary layer, that is valid over uniform flat terrain. On theoretical grounds, it has been seen that for a flow – which is fully in equilibrium with the surface – σ_u / u_* starts from a constant value near the surface and approximately constant within the inner layer, then it achieves a maximum before decreasing linearly with height. At large heights, it is (Harris&Deaves, 1980):

$$\frac{\sigma_u(z)}{u_*} \propto 1 - \frac{z}{h} \tag{2.26}$$

An empirical expression proposed in the H&D model, which matched the data set available to the authors, is:

[1] In the following, the horizontal superscript which distinguishes the mean velocity component $\overline{U}$ from the total velocity in the along wind direction $U = \overline{U} + u'$ is neglected, in order not to burden the treatment. Therefore, in the following it is normally referred to U_m as the mean wind velocity.

$$\frac{\sigma_u(z)}{u_*} = \frac{7.5\left[1-\frac{z}{h}\right]\left\{0.538+0.09\ln\left(\frac{z}{z_0}\right)\right\}^{\left[1-\frac{z}{h}\right]^{16}}}{1+0.156\ln\left(6\frac{h}{z_0}\right)} \tag{2.27}$$

This expression is adopted by the ESDU Data Items (ESDU 85020).

Integral length scales of turbulence

Harris and Deaves also propose an expression for the integral length scale of the longitudinal component of turbulence L_{ux}, which is adopted by the ESDU Data Items (ESDU 85020 and 86010). The length scale increases with increasing height above the ground up to a maximum value. Also, for a given height, it increases with increasing wind speed and surface roughness. As the wind strength increases, the boundary layer height increases and the eddies within the boundary layer are stretched accordingly. Moreover, apart from low levels close to the ground, the longitudinal length scale in the boundary layer is generally twice the value of the lateral scale.

The starting point to develop the H&D model of L_{ux} is to match the well-established Kolmogorov and Von Karman spectrum formulas (Harris and Deaves, 1980). For turbulent flows in which an equilibrium range exists (i.e. at high Re), the Kolmogorov formula for the high frequency range of the spectrum is:

$$nS(z,n) = K_0(\varepsilon U)^{2/3} n^{-2/3} \tag{2.28}$$

being K_o the Kolmogorv parameter.

The Von Karman form of the spectrum for the longitudinal component of turbulence is:

$$\frac{nS(z,n)}{\sigma_u^2} = \frac{4\frac{L_{ux}n}{U}}{\left(1+70.8\left(\frac{L_{ux}n}{U}\right)^2\right)^{5/6}} \tag{2.29}$$

At high frequencies, it reduces to:

$$\frac{nS(z,n)}{\sigma_u^2} = A\left(\frac{L_{ux}\,n}{U}\right)^{-2/3} \tag{2.30}$$

being A = 0.115.
By combining the Von Karman spectrum at high frequencies and the Kolmogorov formula, it is obtained:

$$L_{ux} = \left(\frac{A}{K_o}\right)^{3/2} \frac{\sigma_u^3}{\varepsilon} \tag{2.31}$$

This result is completely independent of the H&D model, which only becomes involved when the variation with height of the standard deviation σ_u (according to equation (2.27)) and the dissipation ε (using equation (2.32)) are introduced. The dissipation can be approximated by:

$$\varepsilon \cong \frac{\tau}{\rho}\frac{dU}{dz} \tag{2.32}$$

Moreover, two further questions are discussed in the H&D model, through the investigation of experimental data:

1. If autocorrelations and spectra are both derived from field measurements, the length scales derived by the integration of the autocorrelation functions are generally greater than the length scales required in the Von Karman formula to fit the measured spectral density data. It is due to the inadequacy of the Von Karman spectrum to represent the characteristic of turbulence closely at all frequencies. The disparity between length scales is a factor of around 1.4, but it decreases with height. A modification to the coefficient A = 0.115 in the formula of the spectrum is then suggested and adopted in (ESDU, 85020):

$$A = 0.115\left[1 + 0.315\,(1 - z/h)^6\right]^{2/3} \tag{2.33}$$

2. Due to anisotropy of turbulence near the ground, the Kolmogorov parameter should vary with height up to a constant value at sufficiently high altitude. An empirical relationship, based on a re-analysis of data by (Thompson, 1990), is defined by equation (2.34) (ESDU, 85020):

$$K_0(z) = 0.19 - \left(0.19 - \frac{0.39}{Ro^{0.11}}\right)\exp\left[-24Ro^{0.155}\left(\frac{z}{h}\right)^{1.24Ro^{0.008}}\right] \tag{2.34}$$

where Ro is the Rossby number ($Ro = u_* / f_c z_0$). By combining equations from (2.31) to (2.34), the expression of the integral length scale of turbulence L_{ux} is thus obtained. Even though the H&D model of L_{ux} is adopted by the ESDU Data Items, it leads to values of the integral length scale which are larger than those recommended in other Codes of practice (e.g. Eurocodes). As a consequence, if the H&D model of L_{ux} is used in the calculations in place of the expressions recommended by other Codes (in case extrapolated at high altitudes), it results that the quasi-static loading is slightly increased, while dynamic loading is decreased.

Cross-correlation functions and cross-spectral densities of wind turbulence

The cross-correlations functions characterize the relationship between fluctuating velocity components at two points in space and in the general case at different times (time lag τ). The zero-lag cross correlations are especially important since they describe how the instantaneous fluctuating component of wind velocity varies in space. Because changes in the gust velocity at one point are not necessarily reflected immediately by similar changes in the gust velocity at another point, the cross-correlation functions are, in general, not symmetrical functions of τ. They can be considered to be composed of two components, the larger one being a symmetrical function of τ and the other being an anti-symmetrical function of τ. Once they are split up in the frequency domain, they are the Fourier transforms of the real (in-phase) and the imaginary (out-of-phase) components of the cross-spectral density. These are the co-spectral density and the quad-spectral density functions, respectively, and are related by the phase-lag angle. The latter is sometimes expressed in terms of an "eddy slope" (ESDU 86010). For most cases, the quad-spectra are small and often neglected, so that the coherence equals the co-coherence. Moreover, the out-of-phase component integrates to zero.

For points having a spatial separation Δx in the along-wind direction, if the assumption of frozen turbulence applies (Taylor's hypothesis), Δx can be converted into an equivalent time lag Δx/U, being U the mean velocity of the flow. In this case, the coherence function would be 1 and the phase angle $\theta = 2\pi n \Delta x / U$. In practice, Taylor's hypothesis is not always strictly applicable (particularly near the ground, when U/n is greater than 300 m, according to an ESDU 86010 recommendation).

The phase angle for separations normal to the wind direction can be taken as zero in the horizontal plane (lateral direction). Instead, for separations in the vertical directions the eddies are inclined with the mean wind shear, so that changes in the gust component higher up are followed by similar changes lower down at some time later. Thus, in general, the phase angles θ_{uu} and θ_{vv} (for the u- and v- wind components) are not zero. They are zero, no matter the value of z and Δz, only in case of isotropic turbulence. This applies to the high frequency range when, even near the ground, turbulent exhibits isotropic properties. However, θ_{uu} and θ_{vv} tend to zero as z increases and dU/dz tends to zero. Because of that, the ESDU 86010 provides the following formulas for the phase angles θ_{uu} and θ_{vv}:

$$\theta_{uu}\{\Delta z\} = \left(1.3\Delta z / z_m\right)(c-1)^{0.7}\left(2\pi n \Delta z / U_m\right) \tag{2.35}$$

$$\theta_{vv}\{\Delta z\} = \left(3\Delta z / z_m\right)(c-1)^{0.7}\left(2\pi n \Delta z / U_m\right) \tag{2.36}$$

where c is a frequency-dependent coefficient defined in the code, that varies between 2 (low frequencies) and 1 (high frequencies). The factors $1.3\Delta z/z_m$ and $3\Delta z/z_m$ are estimations – on the basis of different sources of data up to about 80 m – of the eddy slope for the u and v components.

The H&D model (ESDU Data Items) and other codes: comparison of wind profiles

For purpose of comparison, the H&D model – adopted by the ESDU Data Items and applicable throughout the whole height of the boundary layer – is compared to the extrapolations of the log- and power- law models, adopted by Eurocode and DIN. Rigorously, these would be limited to 200 m and 300 m, respectively. The dependence on latitude is included in the H&D model.

The following case studies are selected:

- terrain category II (z_0 = 0.05 m)

- $V_b(10m) = 25$ m/s
- Latitude $\phi = 30°, 23°$.

In these conditions, according to the Eurocode (up to 200 m), it is:

$$U_m(z) = V_b 0.19 \ln\left(\frac{z}{z_0}\right) \tag{2.37}$$

$$I_u(z) = \frac{1}{\ln\left(\frac{z}{z_0}\right)} \tag{2.38}$$

$$L_{ux}(z) = 300\left(\frac{z}{200}\right)^{0.67 + 0.05\ln(z_0)} \tag{2.39}$$

According to the DIN-EN (up to 300 m), it is:

$$U_m(z) = V_b\left(\frac{z}{10}\right)^{0.16} \qquad I_u(z) = \left(\frac{z}{10}\right)^{-0.16} \qquad L_{ux}(z) = 300\left(\frac{z}{300}\right)^{0.26} \tag{2.40}$$

All the previous models neglect the variation of air density with height. In Backström et al. (2008) the following expression is proposed:

$$\rho(z) = \rho_0 \frac{22000 - z}{22000 + z} \tag{2.41}$$

where $\rho_0 = 1.25$ kg/m^3.

As shown in Figure 2.4, the profiles of mean wind and turbulence intensity recommended by the Codes do not differ significantly at low heights. The H&D model predicts much larger integral scales. This issue is further commented by Harris (1986), because the large values imply, from the structural point of view, an increase in the quasi-static response and a decrease in the dynamic response. The question about the representativeness of such large values is still open today.

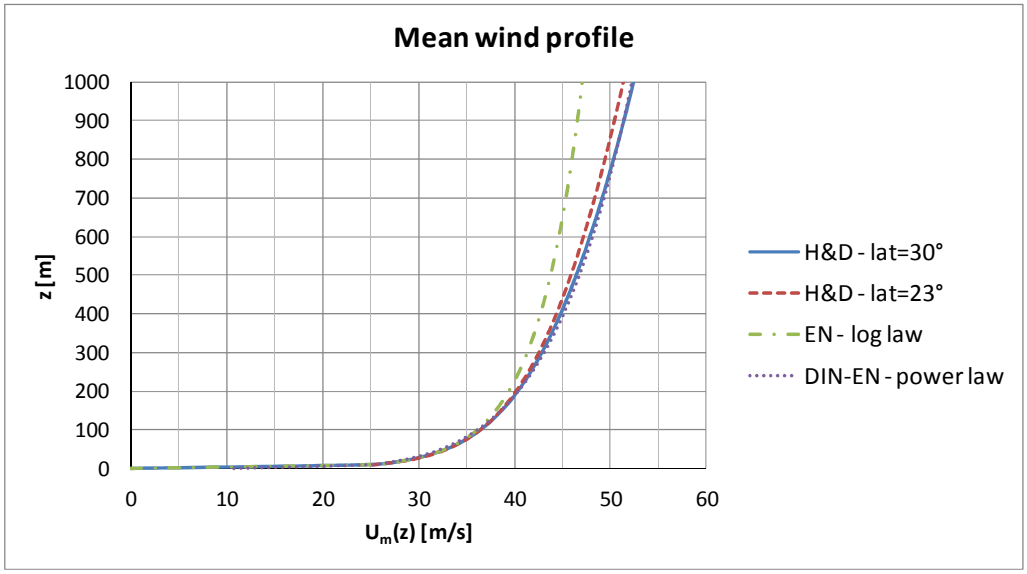

Figure 2.4 Mean wind profile: ESDU, EN, DIN-EN

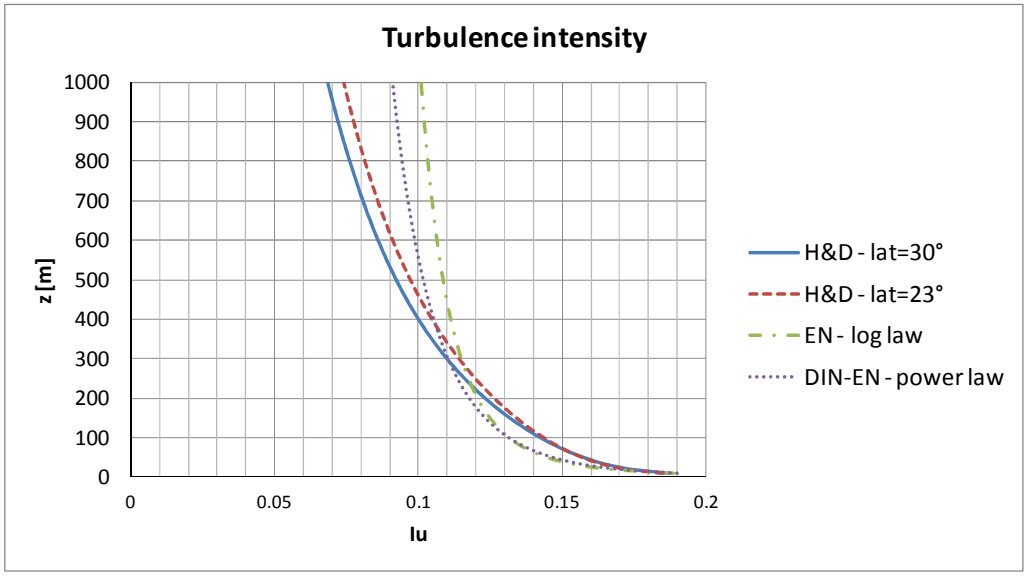

Figure 2.5 Turbulence intensity: ESDU, EN, DIN-EN

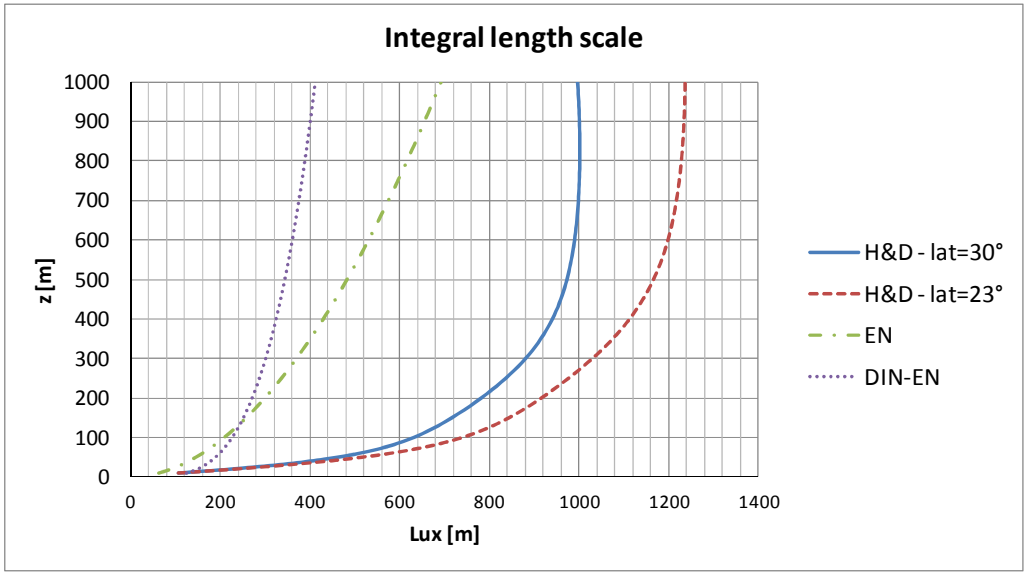

Figure 2.6 Integral length scale: ESDU, EN, DIN-EN

2.3.2 Experimental and numerical investigation of the ABL

Up to around 300 m, wind velocities can be accurately measured at sufficiently high frequency resolution (for example by means of anemometers on high towers, Figure 2.7). Therefore, the structure of wind turbulence up to that level is deeply investigated in literature (Peil et al., 1990, 1992, 1996; Clobes et al., 2009; Clobes&Willecke, 2009).

Figure 2.7 Gartow tower (344 m) equipped with anemometers (picture from http://www.is.tu-braunschweig.de/)

As briefly mentioned in the previous section concerning strong wind conditions, there are still many open problems in the nature of wind at large heights. Recommendations of the Codes of practice are usually limited to 200-300 m. The ESDU Data Items provide profiles which are valid up to the boundary layer height, but there is considerable uncertainty in many parameters, for example the integral length scales of turbulence. Moreover, in light wind conditions the mean wind profile can assume different shapes and no information is currently codified for the designer of super-tall structures. Further investigation in the Ekman layer is thus needed. This section aims at providing an overview of the technologies which are available nowadays to investigate the atmospheric boundary layer at large heights.

Field experiments at large heights

Above 300 m, no experimental evidence is currently available for the purpose of structural wind engineering. It does not mean that no experimental evidence is available at all. In fact, measurements are usually performed at large heights (1000-1500 m) by meteorologists. However, for structural design, specific requirements should be fulfilled:

- sufficiently high frequency resolution, in order to measure turbulence fluctuations;
- spatial averages over big volumes should be avoided;
- relatively small distance between simultaneous measuring points, to calculate cross-correlations.

With regard to the design in the ultimate limit state, only the shear production of turbulence (due to surface friction) and not the buoyancy forces arising from convective motions and thermal stratification of the atmosphere should be considered. It corresponds to neutral stratification of the atmosphere. In these conditions, the scatter of data due to the thermal effects is much reduced, so that a more defined pattern can be evaluated (e.g. power- or log- law for the mean wind profile). Moreover, in the ideal condition of neutral atmosphere, wind is a stationary random process, in the sense that statistics are invariant with time. Instead, thermal effects, convective motions of the atmosphere and buoyancy production of turbulence play a role in light wind conditions. This is a wide field of research in meteorology. For this reason, the instruments that have been used since long time ago to measure wind at large heights are normally required to work only in light wind conditions.
For example, measurements with balloons and aircrafts are possible even at high altitudes. Examples of airborne measurements are reported in Figure 2.8 and Figure 2.9. Such aircrafts do not fly if the wind speed is higher than 10 m/s. In fact, accuracy of these measurements depends on the relative velocity of the aircraft and the wind speed, and it is much affected if they are of the same order.
Balloons represent a less expensive technique than aircrafts for atmospheric investigation. They can be tethered or free balloons. Measurements can be performed either along the vertical while the balloons are flying up, at a fixed point if they are tethered or in the mean wind direction, as they are transported by the flow. Kites are another choice. Again, the use of these instruments by meteorologists is only limited to light wind speeds.

Figure 2.8 Aircraft measurement during the field campaign in Emden, Germany, 2008 (Kroonenberg v.d., 2009)

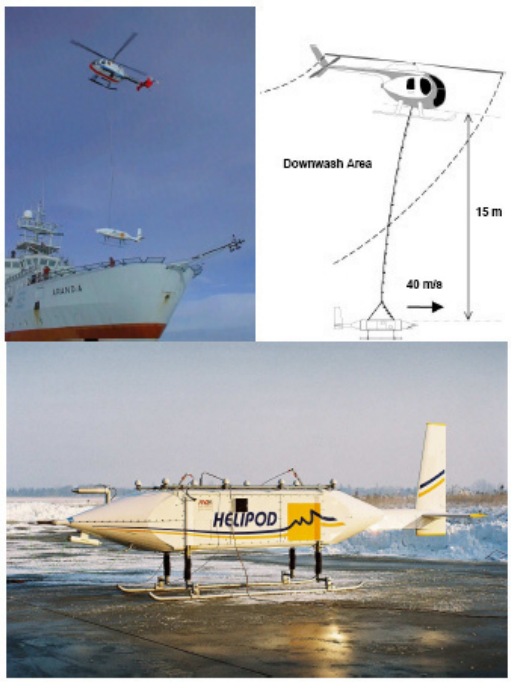

Figure 2.9 Turbulence probe Helipod, field campaign in the Baltic sea (Bange, 2007)

The type of measurements described above fall in the broad category of in-situ sensors, because the sensing instrument (mounted either on towers, aircraft or balloons) lies in the probe volume. Another category is that one of remote sensing instruments. They can be mounted at ground level, on aircrafts or even on satellites. Their peculiarity is that they do not have a sensing element within or around the volume of interest. They infer atmospheric properties through their effects on acoustic, microwave and optical signals propagation through the air. They can be classified into three main groups:

- acoustic waves are used by SODARs (Sonic Detecting And Ranging)
- light waves are used by LIDARs (Light Detecting and Ranging)
- radio waves are used by RADARs (RAdio Detecting And Ranging)

The wind speed is measured through the doppler effects (in fact, the proper names of the instruments would be doppler-SODAR, doppler-LIDAR, doppler-RADAR). The doppler effect consists in the change of frequency between the emitted signal (known and fixed) and the returned signal. The latter depends on the velocity of the air particles which scatter the signal back. This shift in phase is the necessary information to calculate the velocity of air particles, that is the wind velocity.

Figure 2.10. Movable mono-static Doppler SODAR with three antennas for the measurements of mean wind and turbulence profiles (Emeis, 2010)

Some SODAR campaigns have been recently performed (e.g. Tamura et al., 2007), but results are only available for the mean wind up to 500 m. In fact, the main limit of SODARs is that they measure over an averaging time of several minutes (e.g. 30) and the resolution of measurements decreases with height. Thus, it is not possible to have good results above 400-600 m. This height decreases as the wind speed increases, because the backscattered signal tends to be displaced away from the receiver by the wind itself.

RADARs are not addressed in this context since their resolution of wind measurements is low for the scopes of structural engineers. The reason is that the radio wave is not so well aligned. Instead, conceptually similar but much more focused and precise is the light wave used by LIDARs. High frequency measurements are possible with these instruments, thanks to the high speed of light. Moreover, atmosphere can be investigated up to some kilometers, even if with a decreasing resolution as height increases.

Turbulence measurements using lidars are still a subject of research and the method of analysis of data is not fully established, yet. An attempt to answer the question “Can the available wind lidars measure turbulence?” has been recently presented in Sathe et al. (2011).

Conical scanning is the usual mode of operation of a wind LIDAR (see Figure 2.11), in order to measure vertical profiles of the three-dimensional wind vector. In fact, as the signal sweeps around the conical surface, at each altitude several measurements around the circumference are available. They are all needed to provide information about the wind speed at the circumference centre. However, as the height increases, the radius of the circumference increases, so that big horizontal distances are swept at high altitudes, providing information for wind speed only at the circumference centre.

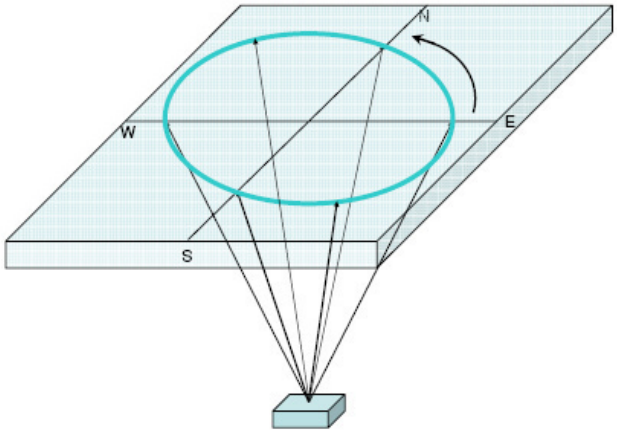

Figure 2.11 Conical scanning pattern of a wind LIDAR in order to measure profiles of the three-dimensional wind vector (Emeis, 2010)

Usually, the signal is transmitted in pulses (Range-resolved remote sensing systems), which are then scattered by atmospheric inhomogeneities or suspensions (e.g., aerosol, droplets), sending a small fraction of the transmitted energy back to the receiver. Distance to the measurement volume is determined by the time of flight of the signal pulse. The state of the art of LIDAR techniques for wind and turbulence measurements by using signal delay for range determination is given by Hardesty & Darby (2005) and Davies et al. (2003). An important point is the spatial resolution, i.e. the volume on which the measured wind speed is averaged. If the signal is sent in pulses in a certain direction, the spatial resolution is related to the distance swept by the pulse in the time interval. Due to the high speed of light, it is in the order of tens of meters (see Figure 2.12). Such a spatial average over big volumes is sometimes useful, for example for applications in the field of wind turbines (Emeis et al., 2007; Mikkelsen et al., 2008). In fact, the average volume is in the order of the volume swept by a blade of a wind turbine, thus it is some good information to design the rotor.

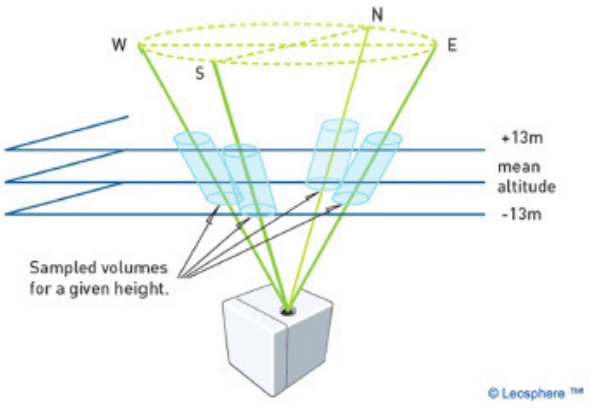

Figure 2.12 Sketch of the operation principle of the Leosphere Windcube (Waechter et al., 2009)

A transportable continuous-wave wind LIDAR (Figure 2.14) has been recently designed and built (Emeis, 2010). The system emits a continuous-wave beam, so that detection of the wind speed at a given range is achieved by focusing, rather than by the time-of-flight method of pulsed systems (range determination by beam focusing). The system cannot distinguish between air motion towards and away from the LIDAR, and this leads to an ambiguity of 180° in the derived value of wind direction. This is easily resolved, however, by making reference to a simple wind direction measurement at a height of a few meters. The profile of the three-dimensional wind vector is yielded by scanning a cone with a 30° half angle once per second (Banakh et al. 1995, Emeis et al. 2007a, Kindler et al. 2007). Hence the diameter of the measured volume is 173 m at a height of 150 m. The probe length increases roughly as the square of the height. As an example, the vertical resolution is ~ ± 10 m at a height of 100 m. Strong reflections from particles and other moving objects outside the focal range (e.g. due to smoke, fog or birds) can lead to spurious Doppler returns (Harris et al. 2001), but these effects can be recognized and mitigated by signal processing techniques.

Figure 2.13 Small pulsed Doppler wind LIDAR for measurement of wind profiles in a height range between 40 and 200 m. Distance determination by pulse travel time (Emeis, 2010)

Figure 2.14 Small continuous-wave Doppler wind LIDAR for measurement of wind profiles in a height range between 10 and 200 m. Distance determination by beam focusing (Emeis, 2010)

Within the context of this dissertation, field measurements have not been available. Moreover, the concern in the Thesis is mainly on strong wind conditions, which so far have never been investigated in any experiment. However, the field of research on full-scale wind measurements at large heights is currently very active and in rapid development. For example, sophisticated mathematical models are being developed to

manage the major and unavoidable problem of spatial average as the height increases (see Emeis, 2010).

Numerical simulations of the atmospheric boundary layer

Numerical simulations of the atmospheric boundary layer are an alternative and a support to field measurements. For example, Canadillas (2010) presents the investigation of the marine boundary layer by means of a PArallelized Large eddy simulation Model (PALM Code), developed at the Institute of Meteorology and Climatology of the Leibniz University of Hannover (Raasch&Etling 1991, 1998 and Raasch&Schröter, 2001). Examples of results achievable with LES are reported in Figure 2.15 and compared to field data (Canadillas, 2010). In this case, the simulation is performed in neutrally stratified conditions of atmosphere. Such conditions are often achieved in the marine boundary layer even at low wind speeds (the ocean surface and the air flowing above it nearly have the same temperature), so that a comparison with field data can be made. However, these well-defined meteorological conditions (no large-scale advection, homogeneous surface, stationary conditions), like over the sea, should not be easily expected over land on heterogeneous terrain, so that such a comparison with observations is generally extremely difficult.

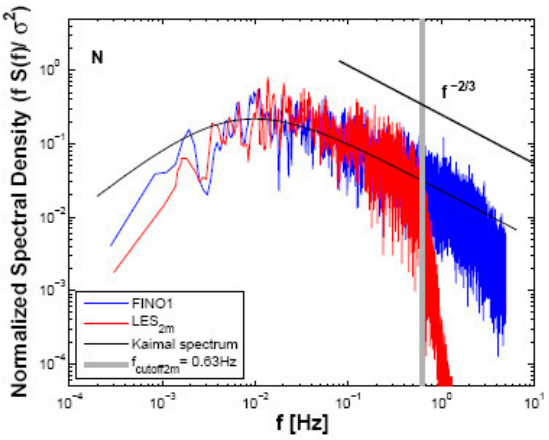

Figure 2.15 Normalized one-dimensional spectra of the horizontal wind velocity fluctuations: comparison between LES simulation of the marine boundary layer (red) and field data (blue) (Canadillas, 2010)

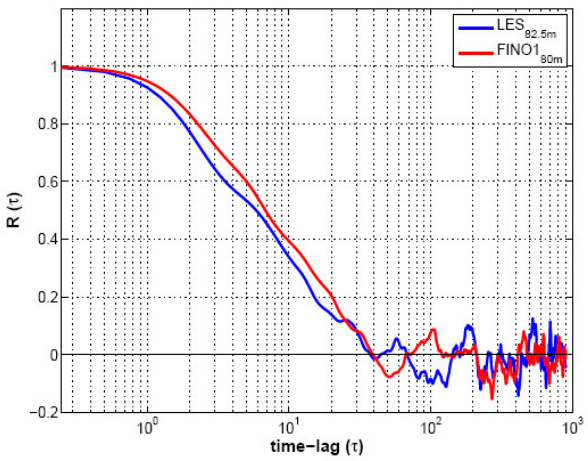

Figure 2.16 Autocorrelation function for the horizontal wind velocity fluctuations: comparison between LES simulation of the marine boundary layer (red) and field data (blue) (Canadillas, 2010)

2.3.3 The Coriolis force

An analytical expression of the Ekman spiral was previously described (equation (2.17)) and a useful approximation to define angle of turn of the mean wind profile is

included in the H&D model (equation (2.25)). However, two further questions need some attention:

1) which is the effect of the Coriolis force on turbulence;
2) which model should be used in tropical regions, where the Coriolis force is small (and becomes zero at the equator). In fact, the H&D model is a mid-latitude model.

These questions are addressed in the following.

The Coriolis force in the equations for turbulent departures

Equations for mean variables in turbulent flow have been previously introduced. In particular, equation (2.7) expresses the conservation of momentum. Turbulent departures of the variables are the deviations from their respective means. The equations for the variance of the wind speed are obtained by expansion of the momentum conservation equation and subtraction of the mean part. Such equations contain the local storage of variance, the advection of variance by the mean wind, the buoyancy production, the shear production, the turbulent transport term describing how variance is moved around by the turbulent eddies, the pressure redistribution term describing how variance is redistributed by pressure perturbations and the viscous dissipation term. The Coriolis term, instead, is identically zero for velocity variances (Stull, 1988).

Phisically, this means that Coriolis force cannot generate turbulence kinetic energy. The Coriolis term merely redistributes energy from one horizontal direction to another. Furthermore, the magnitude of the redistribution term is about three orders of magnitude smaller than other terms. For this reason, the Coriolis terms can be neglected in the turbulence equations, even for the cases where they are not identically zero (Stull, 1988).

The Coriolis force in tropical regions

The equations of motion, which describe all types and scales of atmospheric motions, are derived by the second Newton's law: "the rate of change of momentum of an object referred to coordinates fixed in space equals the sum of all the forces acting". Such forces are: the pressure gradient force, the gravitational force and friction. Moreover, since the motion in the atmosphere is usually referred to a coordinate system rotating with the Earth, the Newton's second law can still be applied provided certain apparent forces: the centrifugal force and the Coriolis force.

The centrifugal force is the force that an object at rest experiences in a rotating system. Usually, its effects are combined with those of the gravitational force, by defining a

gravity force which is everywhere directed normal to the local level. The Coriolis force is the force that a moving object (e.g. an air particle) experiences in a rotating system. Therefore, the Newton's second law for motions relative to a rotating coordinate frame – written in the notation used by Holton (1979) – is:

$$\frac{d\mathbf{V}}{dt} = -2\boldsymbol{\Omega}\times\mathbf{V} - \frac{1}{\rho}\nabla p + \mathbf{F}_r \tag{2.42}$$

The left-hand side represents the substantial derivative of wind flow (local + advective acceleration), while the terms on the right-hand side represent the Coriolis force, the pressure gradient force and the friction force. This is consistent with what has been described before. However, a deeper analysis is required to better understand the flow movements even at low latitudes.

If such an equation is written in spherical coordinates, being x the westward direction, y the northward direction and z the upward direction, it is (Holton, 1979):

$$\frac{du}{dt} - \frac{uv\tan\phi}{a} + \frac{uw}{a} = -\frac{1}{\rho}\frac{\partial p}{\partial x} + 2\Omega v\sin\phi - 2\Omega w\cos\phi + F_x \tag{2.43}$$

$$\frac{dv}{dt} + \frac{u^2\tan\phi}{a} + \frac{vw}{a} = -\frac{1}{\rho}\frac{\partial p}{\partial y} - 2\Omega u\sin\phi + F_y \tag{2.44}$$

$$\frac{dw}{dt} - \frac{u^2+v^2}{a} = -\frac{1}{\rho}\frac{\partial p}{\partial z} - g + 2\Omega u\cos\phi + F_z \tag{2.45}$$

where ϕ is the latitude and a the radius of Earth.

They are the complete equations for all motions in the atmosphere. Now, let us consider the synoptic scale motions, i.e. those systems of typically several hundred kilometers in horizontal direction. Characteristic scales of the field variables based on observed values for mid-latitude synoptic systems are (Holton, 1979):

- U ~ 10 m/s = horizontal velocity scale
- W ~ 10^{-2} m/s = vertical velocity scale
- L ~ 10^{6} m = length scale
- D ~ 10^{4} m = depth scale

- $\Delta p/\rho \sim 10^3$ m^2/s^2 = horizontal pressure fluctuation scale
- $L/U \sim 10^5$ s = time scale

In the free atmosphere, i.e. by neglecting friction, an order-of-magnitude analysis of the equations shows that at mid-latitude the pressure gradient force and the Coriolis force are of the same order of magnitude (10^{-3} m/s^2) and approximately in balance, while all the other terms are one or more orders of magnitude smaller. Thus, the geostrophic approximation – which describes the familiar situation in which the wind blows parallel to the isobars and the Coriolis force balances the pressure gradient force – turns to be confirmed. In other words, being U_g and V_g the horizontal components of the gradient wind, it is:

$$-f_c V_g \cong -\frac{1}{\rho}\frac{\partial p}{\partial x} \tag{2.46}$$

$$+f_c U_g \cong -\frac{1}{\rho}\frac{\partial p}{\partial y} \tag{2.47}$$

At lower altitudes, i.e. within the atmospheric boundary layer (ABL), the equations of motion are approximately a tree-way balance between the pressure gradient force, the Coriolis force and friction (see Figure 2.17 and Figure 2.18).

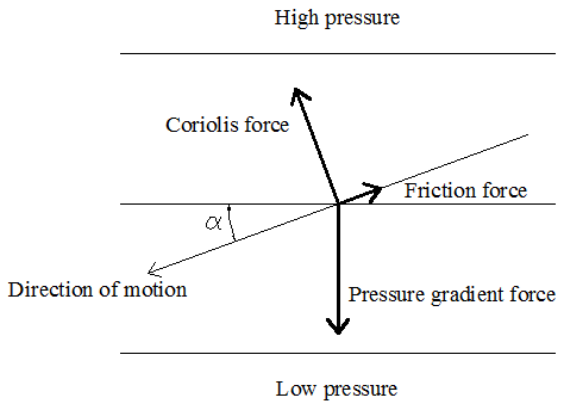

Figure 2.17 Balance of forces within the ABL at mid-latitudes

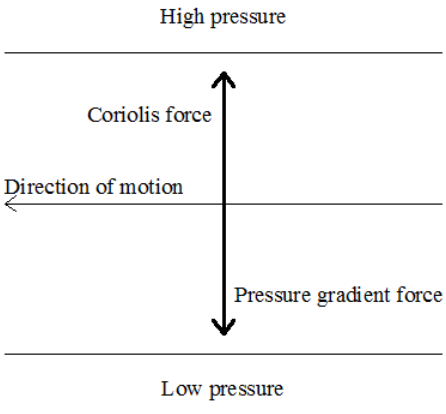

Figure 2.18 Balance of forces in the free atmosphere at mid-latitudes

If the same scale analysis of momentum equations is repeated in tropical regions, it turns out that it is not appropriate to assume that the Coriolis force term balances the pressure gradient. As the Coriolis force becomes smaller, the pressure gradient must be

balanced by the inertial acceleration term. As a consequence, in order to satisfy such a balance, for synoptic scale systems in tropical regions characterized by the same horizontal length and velocity scales as in mid-latitudes, the pressure gradient force is an order of magnitude smaller than at mid-latitudes (Holton, 1979).

Although it is only a rough calculation, it is apparent that large scale motions on the so-called equatorial beta-plane, i.e. in the tropical region including the effect of variation of the Coriolis force with latitude, are much more complicated and result in wave motions involving the balance between pressure gradient forces, inertial forces and a varying Coriolis force (latitude-dependent). Unfortunately, there is not as yet a single unifying theory for tropical motions comparable to the quasi-geostrophic theory for mid-latitude motions. This matter, which was firstly posed by Matsuno in 1966 ("is there quasi-geostrophic motion even at the equator?"), is still of relevance even today in Physics of the Atmosphere (e.g. Verkley&Velde, 2010).

Therefore, for wind engineering purposes, there is no other theory available which includes the effect of the Coriolis force on the mean wind by solving the equations of motion, apart from those proposed for mid-latitude models (e.g. Ekman, 1905 or Harris and Deaves, 1980) and addressed in section 2.3.1. They assume the geostrophic approximation in the free atmosphere, i.e. the balance between the Coriolis and the pressure gradient force. Therefore, the question is: to which extent, in terms of latitude, can we assume that these theories are approximately valid? The answer to this question is as follows: the horizontal frictionless flow can be approximated like geostrophic flow if the inertial acceleration term is sufficiently smaller than the Coriolis force. A convenient measure of the acceleration magnitude compared to the Coriolis force may be obtained by forming the ratio of the characteristic scales for the acceleration and the Coriolis force terms:

$$\frac{U^2 / L}{f_c U} = \frac{U}{f_c L} = Ro \tag{2.48}$$

This ratio is a non-dimensional number called the Rossby number (Ro). Thus, the smallness of the Rossby number is a measure of the validity of the geostrophic approximation. At mid-latitudes (being $U \approx 10$ m/s, $f = 2\Omega\sin\varphi \approx 10^{-4}$ m/s, $L = 10^6$ m), it results $Ro \approx 0.1$. At lower latitude, e.g. 10°, $Ro \approx 0.4$, but only at 4° Ro changes its order of magnitude (≈ 1.0). For this reason, it can be assumed that the geostrophic approximation can be accepted up to a latitude of about 4°. Being on the safe side, the lower limit for latitude can be set at 10° (Houghton, 1977). In view of the solar updraft

tower design, such a limit encloses most of the possible locations for solar towers (see Figure 1.3). It means that the models based on the (frictionless) geostrophic balance can be applied, within an acceptable range of approximation.
However, even if the H&D model approximation is still acceptable at relatively low latitudes, the failure of the model is physically motivated by the different type of storms creating strong winds near the equator, which should be reflected in the design. This issue is addressed by Irwin (2009). The types of storms near the equator tend to be local, e.g. thunderstorms, and in these storms the boundary layer depth is limited by the small scale of the storm and not by Coriolis effects.

2.3.4 **Tropical cyclones and tornadoes**

Tropical cyclones and tornadoes are not included in this work. In these motions the Coriolis force is always of secondary importance with respect to the acceleration term in the equations of motion.
Tropical cyclones (called hurricanes in the Atlantic and typhoons in the Pacific) are intense vertical storms which develop over tropical oceans in regions of very warm surface water. They are characterized by a horizontal scale of the region where convection is strong of about 100 km in radius. Maximum tangential wind speeds in these storms range typically from 50 to 100 m/s. For such high velocities and relatively small scales, the centrifugal force term cannot be neglected compared to the Coriolis force. It means that, to a first approximation, the radial force balance in a steady-state hurricane satisfies the gradient wind relationship (equation (2.49)), but not the geostrophic balance.

$$\frac{U^2}{R} + f_c U = -\frac{1}{\rho}\frac{\partial p}{\partial n} \tag{2.49}$$

Anyway, tropical cyclones rapidly degenerate when they move on land and, as can be seen in Figure 2.19, they do not affect possible locations for solar towers.
Besides tropical cyclones, tornadoes are not considered in this Thesis as well. In fact, a methodology to design structures against tornadoes does not exist. Haan et al. (2008) designed a large tornado simulator for wind engineering applications, but physical model testing in wind tunnels is still in need of further development (Irwin, 2009). Usually, tornadoes are only treated in terms of their probability of occurrence (Goliger&Milford, 1998) and the great majority of structures (with exclusion of nuclear reactors and other critical facilities) is not designed to withstand them.

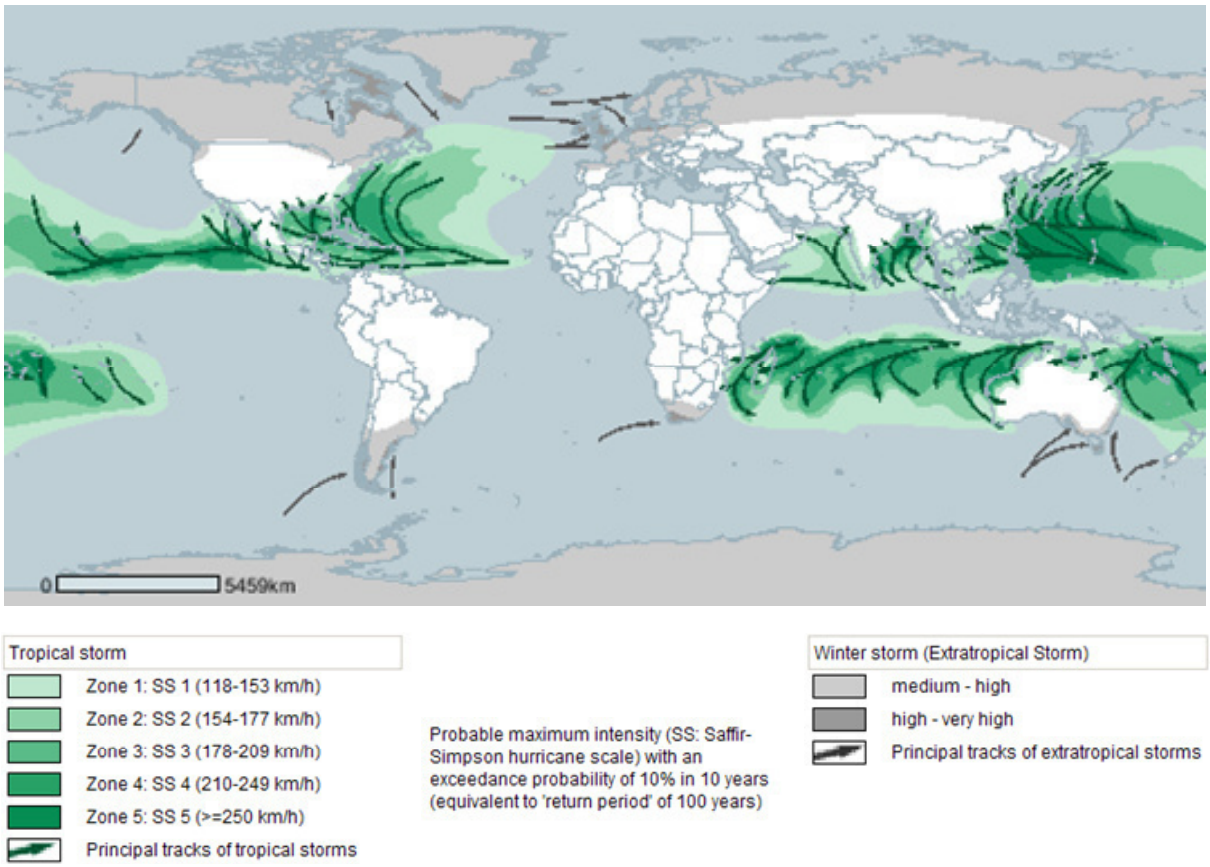

Figure 2.19 Principle tracks and intensities of tropical cyclonic storms

2.4 Structural vulnerability of the tower to the wind action

So far, it is known that the structural vulnerability of the solar tower to the wind action can be significantly reduced by applying stiffening rings along the height (Figure 1.9, Figure 1.12, Figure 1.13). As explained in several publications about solar towers (Goldack, 2004; Backström et al., 2008; Krätzig et al., 2008-2009a,b; Lupi, 2009, 2011; Niemann et al., 2009; Harte et al. 2010; Borri et al., 2010), the stiffening rings guarantee a beam like behaviour at the first eigenmode, reduce ovalling deformations of the shell, increase buckling safety and improve the distribution of internal forces. This is the same concept as for steel chimneys, which was first investigated by Peil&Nölle (1988) and constitutes the basis of the rule in the German Standard DIN 4133.

Figure 2.20 shows the natural vibration modes of the tower depicted in Figure 1.13, that is the reference structure in the Dissertation. The calculation on the left-hand side is done in absence of stiffening rings. The shell-like behaviour (modes with three and two waves, respectively) definitely predominates. Instead, in case of ten stiffening

rings (like those in Figure 1.14), the first vibration mode is a bending mode, with an eigenfrequency of about 0.17 Hz, and the second mode shape is a shell-like one, with two waves and no inversion along the meridian. A wider study about the influence of stiffening rings on the vibration modes can be found in Lupi (2009). It was seen that at least five rings would be necessary along the height, in order to promote a beam-like mode.

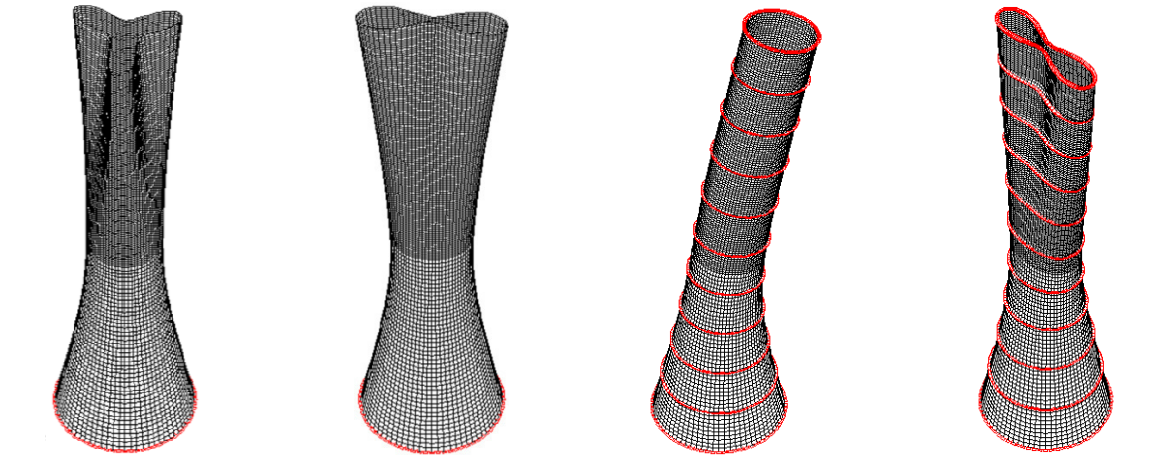

$f_1=f_2$ = 0.073 Hz $f_3=f_4$ = 0.086 Hz $f_1=f_2$ = 0.172 Hz $f_3=f_4$ = 0.311 Hz

Figure 2.20 Natural vibration modes of 1000 m tower (Borri et al., 2010)
without stiffening rings *with 10 stiffening rings*

The reduction of shell-like deformations significantly improves the distribution of internal forces. This diminishes the structural vulnerability, especially to the wind action, because the peaks of tension at the windward side are reduced. Ideally, the internal distribution of forces tends to a beam-like distribution, which is linear in the cross-section and crosses zero at 90°. In presence of ten stiffening rings like those in Figure 1.14, this ideal response distribution is achieved at about middle height of the tower, as shown in Chapter 7 (Figure 7.57). As the peaks of tension due to the wind action are reduced at the windward side, tensile stresses can even be completely balanced by the compressive stresses due to self-weight. Consequently, the amount of steel reinforcement is significantly reduced and if needed it can be restricted to the minimum percentage that is required by the Codes. It was calculated in Niemann et al. (2009) that even at the base of the tower and even at the ultimate limit states, the tensile stresses due to the wind action can be completely balanced by self-weight. This also means that the risk of an overturning of the tower is prevented and pales against overturning are not necessary in the foundations. It explains the relatively small foundation ring, which is depicted below the tower in Figure 1.12 and Figure 1.13.

However, even if the predominant behaviour of the solar tower is a beam-like bending mode, relevant shell stresses still arise, especially in the vicinity of the stiffening rings and in the tip region. The local effects in the vicinity of the stiffening rings are evaluated in Chapter 7. In the tip region, the ovalization of the shell is evident in Figure 7.57, where at high levels compressive forces arise at stagnation and lateral tension is present at the flanges. Therefore, even if the beam-like calculation of the structure provides a good estimation of global effects, it would not be sufficiently representative in view of the design. This is confirmed by Peil&Nölle (1988), who investigated the stress distribution in steel chimneys and proposed a simple formula (introduced in the Eurocodes) to identify the admissible shell geometries, i.e. those geometries that can be calculated by the beam theory. It depends on geometric parameters like H/R and R/t, being H, R and t the height of the tower, the radius and the wall thickness, respectively. The equation for allowable shell geometries is given by Peil&Nölle (1988):

$$\frac{H}{R} \geq 0.14 * \frac{R}{t} + 10 \tag{2.50}$$

In the case of the solar tower, it results (measures are in m):

$$\frac{1000}{75} \geq 0.14 * \frac{75}{0.25} + 10 \quad \rightarrow \quad 13.3 \geq 52 \quad \rightarrow \quad FALSE \tag{2.51}$$

It is then clear that the enhancement of the beam-like behaviour by introducing stiffening rings is a strategy of risk mitigation, because it reduces the structural vulnerability (especially to the wind action), but the design cannot neglect the shell-like behaviour.

In addition, the presence of rings is crucial in order to reduce the structural vulnerability to vortex shedding. The frequency of shedding (n_s) is conveniently represented in non-dimensional form by the Strouhal number:

$$S_t = \frac{n_s D}{U} \tag{2.52}$$

where D is the diameter of the cylinder and U is the wind speed. For circular cylinders, S_t is of the order of 0.18-0.2 (but it varies with the Reynolds number). As wind speed increases, the dominant frequency of vortex shedding n_s increases, until the critical flow velocity U_{cr} is reached. It happens when n_s is close to a natural frequency of vibration of the body. At the critical flow speed, a significant amplification of the across-flow forces occurs and large amplitude of across-flow oscillations can result.
The amplitude of the induced oscillations depends on the Scruton number:

$$S_{cr} = \frac{4\pi m_{i,e} \xi_i}{\rho D^2} \tag{2.53}$$

where $m_{i,e}$ is the equivalent mass of the structure per unit length corresponding to the i^{th} mode of vibration and ξ_i is the damping ratio corresponding to the i^{th} mode of vibration. If the Scruton number is large, the motion induced by the vortex shedding will not exceed a few per cent of the diameter, although fluctuating forces induced by vortex shedding will still be present. Instead, if the Scruton number is small, the motion of the body has a significant influence on the strength of the vortices shed and the forces induced by them, which in turn affect the oscillation amplitude. It is an aeroelastic effect.
When the amplitudes of oscillation are small, the fluctuating forces are generally random in nature, with significant energy distributed over a relatively broad band of frequencies centered on n_s. In this case, the distribution of the vortex-induced fluctuating forces along the length of the cylinder is also disorganized, which means that the maximum value of the fluctuating force does not occur simultaneously at all positions along the cylinder. The resulting response is a broad-band response of random amplitude nature at approximately the body frequency. For larger amplitudes of oscillation, the local forces due to vortex shedding are amplified. In such cases, the motion of the structure tends to cause the shedding frequency n_s to “lock-in” to the body frequency n_j over a range of local flow velocities. The fluctuating forces at various sections along the structure in the lock-in region are in phase with the body motion and thus completely correlated with each other, further enhancing the response. These forces are nearly periodic in nature, with significant energy confined to a relatively narrow band of frequencies centered on the body frequency n_j. The resulting response is a narrow-band response of an almost constant amplitude of sinusoidal nature at approximately the frequency n_j.

Solar towers are characterized by small Scruton numbers, therefore the lock-in phenomenon may be dangerous. However, the critical wind speed at which it would occur is so high that, in practice, it cannot be reached. It is primarily due to the aspect ratio of solar towers, which is generally not too high. It reduces the sensitivity to vortex-induced oscillations. In addition, the presence of the ring beams along the height is very important, because the beam-like behaviour at the first eigenmode increases the critical velocity, as calculated in the following.
The critical wind speed for 1-kilometer tall tower with ten stiffening rings (n_1 = 0.17 Hz), corresponding to a beam-like bending mode, is calculated as (by assuming D = 150 m, like in Figure 1.13 at the tower top):

$$U_{cr} = \frac{n_1 D}{S_t} = \frac{0.17*150}{0.20} = 127.5 \text{ m/s} \tag{2.54}$$

As regards the ovalling modes of vibration, the critical wind speed corresponding to the second mode, characterized by two waves around the cross-section (n_1 = 0.31 Hz), can be calculated as:

$$U_{cr} = \frac{n_2 D}{2S_t} = \frac{0.31*150}{2*0.20} = 116.25 \text{ m/s} \tag{2.55}$$

The Codes require that the critical wind speed is at least 25% higher than the design wind speed, assumed for a period of 50 years. Such requests are largely satisfied. However, in absence of rings (or with a few rings, like one or two, see Lupi (2009)), the critical velocity would be much lower. For example, if n_1 = 0.073 Hz and there are three waves, like in Figure 2.20, the critical velocity would have been only 18 m/s. In this case, the amount of steel reinforcement and width of cracks are secondary aspects, because the collapse of the structure would likely be produced by aeroelastic effects due to the lock-in.